Imaging of Pediatric Growth Plate Disturbances[1]

Jie C. Nguyen, MD, MS
B. Keegan Markhardt, MD
Arnold C. Merrow, MD
Jerry R. Dwek, MD

Abbreviations: GRE = gradient recalled echo, SOC = secondary ossification center, ZPC = zone of provisional calcification

RadioGraphics 2017; 37:1791–1812

https://doi.org/10.1148/rg.2017170029

Content Codes: MK MR PD

[1]From the Department of Radiology, University of Wisconsin School of Medicine and Public Health, Madison, Wis (J.C.N., B.K.M.); Department of Radiology, Cincinnati Children's Hospital Medical Center, Cincinnati, Ohio (A.C.M.); and Department of Radiology, University of California at San Diego, Rady Children's Hospital and Health Center, San Diego, Calif (J.R.D.). Presented as an education exhibit at the 2016 RSNA Annual Meeting. Received March 1, 2017; revision requested May 11 and received May 17; accepted June 7. For this journal-based SA-CME activity, the author A.C.M. has provided disclosures (see end of article); all other authors, the editor, and the reviewers have disclosed no relevant relationships. **Address correspondence to** J.C.N., Department of Radiology, Hospital for Special Surgery, 535 E 70th St, New York, NY 10021 (e-mail: *jiec29@gmail.com*).

SA-CME LEARNING OBJECTIVES

After completing this journal-based SA-CME activity, participants will be able to:

- Identify the normal anatomy and physiologic features of the primary growth plate complex.
- Recognize the various imaging findings commonly associated with direct and indirect injuries to the primary growth plate.
- Understand the goals of imaging and various treatment approaches.

See www.rsna.org/education/search/RG.

The growth plates, or physes, are visible on virtually all images obtained in skeletally immature children. The proper function of these growth plates depends on an intricate balance between chondrocyte proliferation, which requires nourishment from the epiphyseal vessels, and chondrocyte death, which requires the integrity of the metaphyseal vessels. Therefore, injury to the growth plate (ie, direct insult) or vascular compromise on either side of the growth plate (ie, indirect insult) can cause growth plate dysfunction. Direct growth plate insults occur most commonly with Salter-Harris fractures, and injuries that allow the transphyseal communication of vessels are at a higher risk for subsequent transphyseal bone bridge formation. Indirect insults lead to different sequelae that are based on whether the epiphyseal blood supply or metaphyseal blood supply is compromised. Epiphyseal osteonecrosis can result in slowed longitudinal bone growth, with possible growth plate closure, and is often accompanied by an abnormal secondary ossification center. In contrast, the disruption of metaphyseal blood supply alters endochondral ossification and allows the persistence of chondrocytes within the metaphysis, which appear as focal or diffuse growth plate widening. Imaging remains critical for detecting acute injuries and identifying subsequent growth disturbances. Depending on the imaging findings and patient factors, these growth disturbances may be amenable to conservative or surgical treatment. Therefore, an understanding of the anatomy and physiologic features of the normal growth plate and the associated pathophysiologic conditions can increase diagnostic accuracy, enable radiologists to anticipate future growth disturbances, and ensure optimal imaging, with the ultimate goal of timely and appropriate intervention.

Introduction

Bone formation occurs by way of intramembranous and endochondral ossification. In general, flat bones develop by means of intramembranous growth and long bones develop by means of endochondral growth. With intramembranous growth, bone formation occurs directly from the mesenchyme. With endochondral growth, bone formation occurs on a cartilaginous framework at the growth plate (1,2).

Primary "discoid" and secondary "spherical" growth plates are found at the ends of long bones. The primary growth plate is responsible for the longitudinal growth of the bone. This growth plate is bound peripherally by the fibrous perichondrium. The secondary growth plate, or acrophysis, is responsible for the enlargement of the secondary ossification center (SOC) within the cartilaginous epiphysis and is the only growth center in smaller bones, such as the apophyses, carpal and tarsal bones, and sesamoid bones (1) (Fig 1).

The primary growth plate is a critical component of the immature skeleton. Impairment and dysfunction of this structure can result in

TEACHING POINTS

- Primary "discoid" and secondary "spherical" growth plates are found at the ends of long bones. The primary growth plate is responsible for the longitudinal growth of the bone. This growth plate is bound peripherally by the fibrous perichondrium. The secondary growth plate, or acrophysis, is responsible for the enlargement of the secondary ossification center (SOC) within the cartilaginous epiphysis.
- For proper function of the primary growth plate, the zonal arrangement and cellular function must be orderly and the vascular supply from the adjacent epiphysis and metaphysis must be intact. Injury to either the growth plate (direct injury) or the adjacent epiphysis and metaphysis (indirect injury) can lead to growth plate dysfunction and future growth disturbance.
- For type IV Salter-Harris fractures, surgical restoration of the joint surface realignment is often required, and these injuries are more worrisome owing to the potential for transphyseal vascularity, which facilitates the recruitment of osteoprogenitor cells and thus leads to subsequent bridge formation.
- Epiphyseal osteonecrosis can cause indirect growth plate dysfunction and thus lead to a combination of characteristic findings with variable degrees of severity, such as an abnormal SOC, slowed longitudinal growth, and/or bridge formation.
- Metaphyseal vascular compromise leads to prolonged survival of hypertrophic chondrocytes, producing lengthening of the chondrocyte columns, which can appear as growth plate widening.

lifelong morbidity, including limb length discrepancy, angular deformity, and altered joint biomechanics. However, the exact clinical implications of the growth disturbance depend on the anatomic location, the severity of the deformity, and the remaining growth potential. For example, disturbances that involve the weight-bearing lower extremities in younger children are less well tolerated, are more likely to require intervention, and more often result in early osteoarthritis and joint replacement.

For proper function of the primary growth plate, the zonal arrangement and cellular function must be orderly and the vascular supply from the adjacent epiphysis and metaphysis must be intact. Injury to either the growth plate (direct injury) or the adjacent epiphysis and metaphysis (indirect injury) can lead to growth plate dysfunction and future growth disturbance. The most common insult mechanism is trauma, which can directly or indirectly injure the growth plate. Less common mechanisms include vascular compromise, infection, inflammation, radiation, and tumor (3); these insults are more likely to primarily affect the epiphysis and metaphysis and only indirectly injure or secondarily involve the growth plate. Indirect insults may cause very different sequelae based on whether the epiphyseal blood supply or metaphyseal blood supply is compromised.

In this article, we review the normal anatomy and physiologic features of the primary growth plate complex—which comprises the growth plate, epiphysis, and metaphysis—and the pathophysiology of direct and indirect insults. The common imaging findings of growth disturbance such as bone bridge, differential longitudinal growth, and growth plate widening are also described. Best examples are provided to illustrate the various injury patterns; however, multiple patterns often coexist, as most insults affect more than one component of the growth plate complex. Finally, the roles of imaging and rationales for treatment are addressed. This review is focused on events that involve the primary growth plate at the ends of long bones because it has been more thoroughly studied. Although we review the development and normal anatomy of the secondary growth plate, an in-depth discussion of the pathologic processes that affect this structure is beyond the scope of this article.

Primary Growth Plate Complex

During the 6th week of embryonic development, mesenchymal cells differentiate into chondrocytes that are responsible for the formation of a cartilaginous model of the future skeleton. In the central portion of this cartilaginous anlage (future diaphysis), the chondrocytes hypertrophy and the matrix begins to calcify. During the 7th week, a periosteal sleeve forms. At the end of the 8th week, vascular invasion brings mesenchymal cells that differentiate into osteoblasts and osteoclasts (4). Osteoblasts manufacture an osteoid matrix on the calcified matrix to produce the primary ossification center, while the osteoclasts are responsible for bone remodeling and formation of the medullary cavity. As the primary ossification center grows and expands bidirectionally toward the ends of the bone, its leading edges become the primary growth plates (5,6). In the following sections, we review the *(a)* zonal anatomy and function of the growth plate, *(b)* normal anatomy and maturation of the epiphysis, and *(c)* endochondral ossification and vascular anatomy of the metaphysis (Fig 1).

Growth Plate

At birth, the primary growth plates are relatively smooth and flat. Growth plate undulation increases with age in response to physiologic dynamic biomechanical forces (7,8). During childhood, the thickness of the growth plate remains relatively constant because of an intricate balance between chondrocyte proliferation and death. Narrowing across the growth plate signals its closure and impending skeletal maturation. Closure starts at sites of major undulations, which occur centrally in the distal femur and proximal tibia but at the anteromedial Kump bump in the distal tibia. The final conversion of chondrocytes into bone leaves

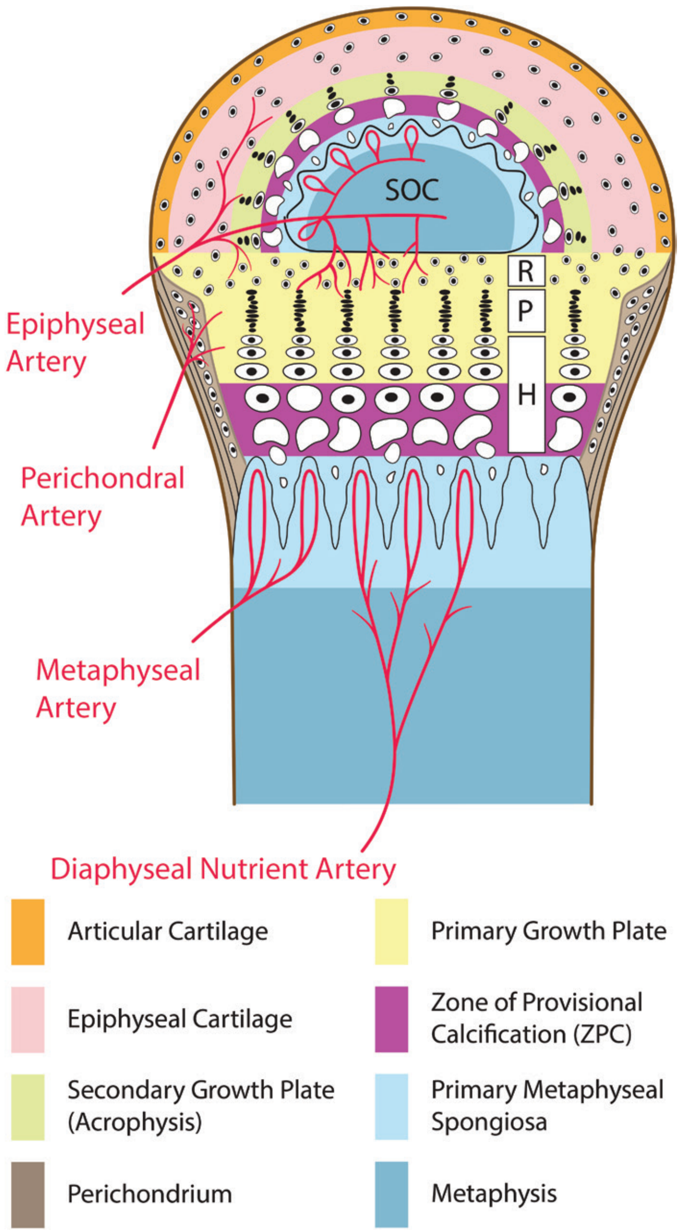

Figure 1. Drawing illustrates the anatomy at the end of a long bone (not drawn to scale). The distal ends of a long bone in a child contain cartilage and bone. There are three types of hyaline cartilage at this level: superficial articular cartilage, centrally located epiphyseal cartilage, and growth plate cartilage. The primary growth plate is responsible for longitudinal growth of the bone, while the secondary growth plate is responsible for the enlargement of the secondary ossification center (SOC), which ultimately provides shape to the proximal and distal ends of bones. Both growth plates contain chondrocytes arranged in zones: randomly distributed reserve cells *(R),* linearly arranged proliferative cells *(P),* and enlarged hypertrophic cells *(H)* that undergo apoptosis at and near the zone of provisional calcification (ZPC). Within the primary metaphyseal spongiosa, calcified cartilage is replaced by laminar bone. The epiphyseal vessels often arise from the periosteum, travel in epiphyseal vascular channels, and nourish the reserve and upper proliferative zones. The metaphyseal vascular loops arise from terminal branches of central nutrient and peripheral metaphyseal vessels and terminate just proximal to the ZPC, leaving the hypertrophic zone relatively avascular. The perichondrium is responsible for the peripheral growth and provides support to the primary growth plate. The perichondrial vessels also supply the periphery of the growth plate, leaving the central growth plate relatively vulnerable to ischemic injury.

behind a physeal scar, which represents a residual zone of provisional calcification (ZPC) (2), leftover horizontal trabeculae at the site of the prior ZPC, or a combination of these entities. This process is often observed within a few years after the closure of the growth plate, but it can (rarely) persist into adulthood (9) (Fig 2).

At histologic analysis, the growth plate is found to be highly cellular (up to 75% by volume), with chondrocytes maturing as they move from the epiphyseal side toward the metaphysis (10). Three distinct zones of chondrocytes are recognized based on their microscopic cellular morphology and function: reserve, proliferative, and hypertrophic zones (Fig 1). It should be noted that we grouped ZPC within the hypertrophic zone (4,5).

Reserve Zone.—The reserve (germinal) zone contains an abundant extracellular matrix, disorganized collagen fibrils, and randomly distributed chondrocytes. These chondrocytes are responsible for storing nutrients (glycogen and lipids) and divide only sporadically. The oxygen tension at this level is low (5).

Proliferative Zone.—In contrast, in the proliferative zone, collagen fibrils are confined to longitudinal septa and chondrocytes are organized into columns (5). These chondrocytes divide rapidly and contribute to the lengthening of the bone. The results of tritiated thymidine autoradiographic studies (4,5) suggest that the top cell of each column is the true progenitor cell. The oxygen tension is the highest in this zone, facilitating

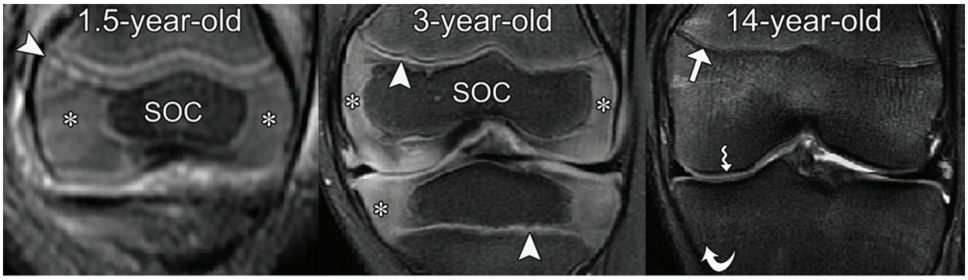

a.

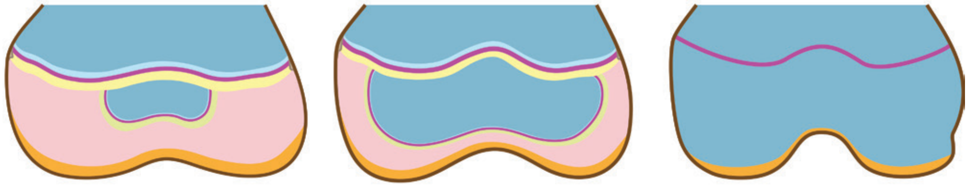

b.

Figure 2. Normal sequence of bone maturation in three children of different ages. Coronal fluid-sensitive magnetic resonance (MR) images in two boys (left and middle) and a girl (right) **(a)** and corresponding illustrations **(b)** show that the epiphyses (* in **a**) are initially partially or completely cartilaginous but then are rapidly and progressively replaced by the enlarging SOC until only the articular cartilage (wavy arrow in **a**) remains. The thickness of the primary growth plate (arrowheads in **a**) stays relatively constant during development. At the onset of skeletal maturation, the growth plate narrows and becomes less hyperintense (straight arrow in **a**) and then finally closes completely; however, it can leave behind a physeal scar (curved arrow in **a**) temporally. Refer to the color key in Figure 1.

robust aerobic metabolism and mitochondrial uptake of calcium. The oxygen and nutrient supply comes from branches of the epiphyseal artery, which course within vascular channels through the reserve zone to nourish the upper proliferative zone (5). Animal study results (11) have shown that insult to this zone is likely to result in growth disturbance.

Hypertrophic Zone.—The hypertrophic zone prepares the matrix for calcification and triggers organized chondrocyte death (ie, apoptosis). This zone can be subdivided into the zones of maturation, degeneration, and provisional calcification (4,5). Chondrocytes become depleted of glycogen, enlarge (up to fivefold), and undergo vacuolation. The vacuolation process leads to the production of cytoplasmic "holes," induces nuclear fragmentation, and causes loss of cell membrane integrity. The metaphyseal arterial loops are found just short of the ZPC, leaving the hypertrophic zone avascular. Therefore, the oxygen tension is reduced by half and thus leads to anaerobic metabolism and mitochondrial release of calcium, facilitating matrix calcification. Initially, calcification occurs along the longitudinal septa. Further accumulation of calcium salt deposits causes the creation of amorphous areas containing calcium phosphate, which give way to hydroxyapatite crystals that coalesce along the ZPC. This progressive matrix calcification hinders the diffusion of nutrients and oxygen, further ensuring apoptosis of the remaining chondrocytes (5).

Perichondrium.—The perichondrium surrounds the periphery of the growth plate and contains the ossification groove of Ranvier and the ring of LaCroix. The groove of Ranvier is wedge shaped, surrounds the periphery of the growth plate, and is responsible for the transverse (latitudinal) growth of the growth plate. The ring of LaCroix is a dense fibrous band that provides mechanical support to the chondro-osseous junction and is continuous with the periosteum (5,12). Similar to the periosteum, the perichondrium is hypointense with all MR imaging pulse sequences. In contrast to the periosteum, however, the perichondrium is tightly attached to the underlying growth plate, acting as a barrier to the epiphyseal spread of metaphyseal subperiosteal pathologic processes (13,14). The perichondral vessels supply the perichondrium and most peripheral aspects of the growth plate (Fig 1), making the central growth plate relatively vulnerable to insult. This vulnerability accounts for the "cupping" deformity that can result from ischemia (15) (Fig 3).

Epiphysis

During the perinatal period, the epiphysis is typically entirely cartilaginous, consisting of peripheral avascular articular hyaline cartilage and central vascularized nonossified epiphyseal hyaline cartilage. The epiphyseal nutrient vessels arise from periosteal vessels, travel in vascular channels (16), and are initially oriented along the long axis of the bone, with some channels extending across the growth plate into the metaphysis. These trans-

Injury Type	Mechanism and Resultant Imaging Findings	Illustration of Possible Imaging Findings*	Example Injuries†
Direct	Mechanism: transphyseal vascularity facilitates recruitment of osteoprogenitor cells and subsequent bridge formation Imaging findings: bone bridge, delayed cupping deformity	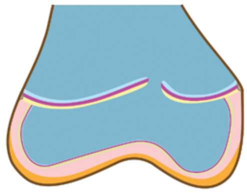	Salter-Harris fractures Slipped capital femoral epiphysis
Indirect (epiphyseal)	Mechanism: epiphyseal vascular compromise leads to injury of the epiphysis and, if severe enough, the adjacent juxtaepiphyseal growth plate (reserve and upper proliferative zones), producing a spectrum of findings Imaging findings: small fragmented SOC, slowed longitudinal growth, focal bridge or diffuse growth plate closure	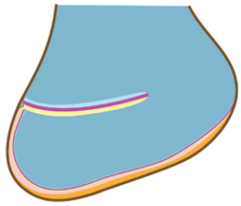 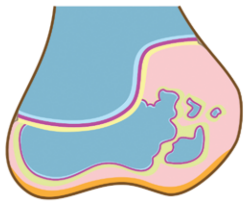	Legg-Calvé-Perthes disease Osteonecrosis following DDH treatment with hyperabduction Fishtail deformity Tibia vara (Blount disease) Epiphyseal osteonecrotic osteomyelitis
Indirect (metaphyseal)	Mechanism: metaphyseal vascular compromise disrupts endochondral ossification, allowing chondrocytes to extend into the metaphysis Imaging findings: diffuse band from repetitive microtrauma, focal tongue from single or limited number of insults	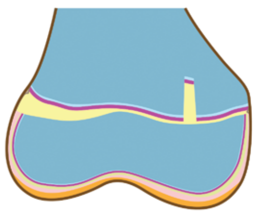	Metaphyseal corner fractures Metaphyseal osteonecrosis Overuse injury Insensitivity to pain with recurrent injuries

Figure 3. Causal mechanisms and stereotypical imaging findings of direct and indirect injuries of the growth plate. *Refer to the color key in Figure 1. †Although predominant patterns are presented, many cases involve more than one component of the growth plate complex. *DDH* = developmental dysplasia of the hip.

physeal channels disappear by the time a child is 12–18 months of age (17). Immediately before the formation of the SOC, vascular channels coalesce centrally and take on a radial pattern of orientation (18) (Fig 4). This causes local chondrocytes to hypertrophy and release metalloproteinases (gelatinase B and collagenase-3) that break down the cartilaginous matrix (19), which subsequently becomes calcified and ossified (6).

The newly ossified SOC is initially spherical and is surrounded by an acrophysis with chondrocytes arranged in a zonal pattern that is analogous to their pattern in the primary growth plate (Fig 1). The portion of the acrophysis that faces the primary growth plate closes first, producing a hemispheric SOC. With time, the acrophysis expands toward the periphery, replacing the nonossified epiphyseal cartilage so that at skeletal maturation, only the articular cartilage remains (5,6) (Fig 2). The MR imaging signal intensity of the SOC is based on the marrow content of this center, which initially comprises hematopoietic red marrow that is mildly hyperintense relative to muscle on T1-weighted MR images and hyperintense on fluid-sensitive MR images. However, within 6 months of the radiographic appearance of the SOC, the marrow converts to fatty yellow marrow that is markedly hyperintense on T1-weighted MR images (20). As the SOC grows along its peripheral margin, the marrow conversion proceeds in a central to peripheral direction. A comprehensive review of the pathologic entities associated with the acrophysis is beyond the scope of this review.

Metaphysis

The main functions of the metaphysis are cartilaginous matrix removal, bone formation, and metaphyseal spongiosa remodeling (4). The primary spongiosa abuts the ZPC and contains calcified cartilage but little to no bone. One to two cells from the ZPC, endochondral ossification occurs, with osteoblasts laying down bone on

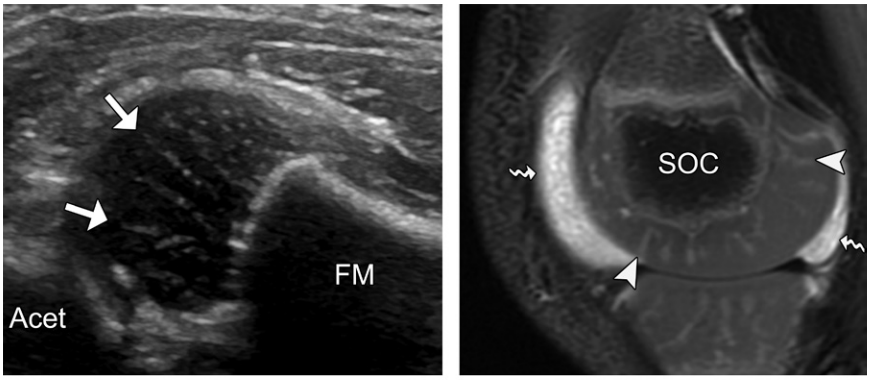

a. b.

Figure 4. Epiphyseal vascular channels. **(a)** Longitudinal gray-scale ultrasonographic (US) image of the right hip in a 2-month-old boy with developmental dysplasia of the hip shows normal parallel orientation of the vascular channels (arrows) along the long axis of the bone. On histologic specimens (not shown), some of these channels extended across the growth plate into the metaphysis. *Acet* = acetabulum, *FM* = femoral metaphysis. **(b)** Sagittal contrast material–enhanced T1-weighted fat-saturated MR image of the knee of a 3-year-old girl with juvenile idiopathic arthritis shows the convergence of vascular channels (arrowheads) onto the SOC. The inflammation associated with uncontrolled arthritis makes these channels particularly conspicuous. Thick enhancing synovitis (wavy arrows) also is present.

calcified cartilaginous bars. The adjacent secondary spongiosa is responsible for internal and external remodeling. Internal (histologic) remodeling entails the removal of cartilaginous bars and the replacement of lamellar bone. External (anatomic) remodeling involves peripheral remodeling that leads to funnelization of the metaphysis (5). The metaphyseal blood supply is derived from a combination of centrally located branches that originate from the diaphyseal nutrient artery and contribute roughly 80% of the blood supply, and peripherally located metaphyseal vessels that penetrate the metaphysis and contribute roughly 20% of the blood supply (3). These vessels form terminal vascular loops and capillary tufts within the spongiosa (5) (Fig 1). Localized vascular stasis predisposes this area to hematogenous deposition of disease and ensures a low oxygen tension environment (4).

At MR imaging, the signal intensity of the metaphysis, with the exception of the primary spongiosa, reflects the composition of the underlying bone marrow. The physiologic conversion of red marrow to yellow marrow occurs throughout life, but it progresses at a more rapid pace during childhood. In the long bones, marrow conversion starts in the epiphyses and apophyses, continues in the diaphyses, and is finally completed in the metaphyses—with conversion in the distal metaphysis occurring slightly earlier than that in the proximal metaphysis. Systemic stress can induce the reconversion from yellow marrow to red marrow in the exact opposite order. Therefore, it is not uncommon to encounter residual red marrow in the metaphyses of children, young adults, and those recovering from systemic stressors (21). In contrast, the primary spongiosa contains more cartilage than bone and is therefore hyperintense on fluid-sensitive MR images.

Growth recovery lines, also known as growth arrest lines, reflect the integrity of the underlying growth plate. These lines are commonly found within the metaphysis and represent thickened, horizontally oriented trabeculae that form as a result of a temporary slowdown of longitudinal cartilage growth during a time of stress. These lines are thickest and most obvious when they are newly formed and within more rapidly growing metaphyses, such as those of the distal femur and proximal tibia (22). With time, these lines are displaced toward the diaphysis, remodeled, and finally disappear as metaphyseal bone converts to diaphyseal bone. Symmetric growth results in lines that parallel the contour of the adjacent growth plate. An angled or obliquely oriented growth recovery line indicates tethering by an underlying transphyseal bridge, and continued growth will lead to progressive angulation deformities. Isolated growth recovery lines in the fibula or ulna increase the possibility of diffuse premature growth plate closure of the ipsilateral tibia and radius, respectively. Growth recovery lines are typically dark on all MR images and are best visualized against a background of bright yellow marrow on non–fat-saturated MR images (Fig 5). These lines are often radiographically evident 6–12 weeks after the injury (23), which precedes a detectable bridge that typically occurs after 3 months (3). Research has shown that MR imaging outperforms radiography for earlier visualization of these lines by up to 6–7 weeks (24).

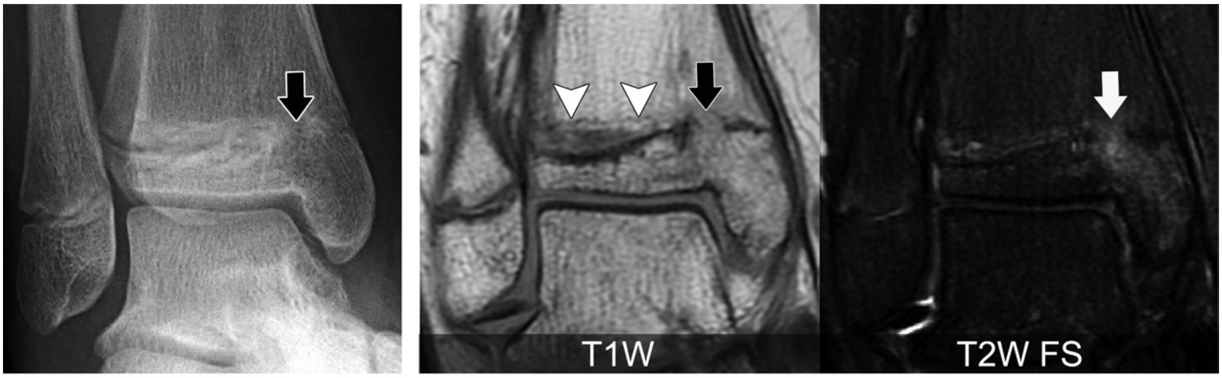

a. b.

Figure 5. Growth plate bridge in a 13-year-old boy 8 months after a type IV Salter-Harris fracture. **(a)** Oblique ankle radiograph shows focal loss of the normal growth plate lucency at the Kump bump (arrow), a recognized site of major undulation of the distal tibial primary growth plate. **(b)** Findings on coronal T1-weighted *(T1W)* and T2-weighted fat-saturated *(T2W FS)* MR images confirm the presence of a small osseous bridge (arrows) crossing the physis, with adjacent focal bone marrow edema resulting from altered biomechanics. Note the angled growth recovery line (arrowheads), which results from asymmetric longitudinal growth between the medial and lateral portions of the distal tibial growth plate due to tethering at the bridge.

Imaging of Hyaline Cartilage

MR imaging is the preferred imaging modality for evaluating hyaline cartilage, which is radiolucent on radiographs and hypoattenuating on computed tomographic (CT) images. Hyaline cartilage is mainly composed of water (70% by volume) and a solid matrix that consists primarily of type II collagen and large aggregating proteoglycan macromolecules. Therefore, hyaline cartilage is isointense on T1-weighted MR images and hyperintense on fluid-sensitive MR images, such as T2-weighted fat-saturated and short tau inversion-recovery (STIR) images.

Growth plate cartilage, epiphyseal cartilage, and articular cartilage are different types of hyaline cartilage and can be distinguished from each other on the basis of their different locations and signal intensities at fluid-sensitive and contrast-enhanced MR imaging (13) (Fig 6). At T2-weighted MR imaging, articular cartilage and growth plate cartilage are relatively more hyperintense than the adjacent epiphyseal cartilage, because articular cartilage has more organized collagen fibrils (2) and the water in growth plate cartilage is less tightly bound to macromolecules (25). Lengthening the echo time can further decrease the epiphyseal cartilage signal intensity and increase the contrast between epiphyseal cartilage and growth plate cartilage (25). Following contrast material administration, growth plate cartilage shows earlier and more pronounced enhancement compared with epiphyseal cartilage. Owing to the unique vascular channel anatomy of the epiphyseal cartilage, three distinct phases of enhancement are observed: vascular, canalicular, and cartilaginous enhancement, with the latter phase occurring after 5–10 minutes (18,26). The progressive involution of the vascular channels with increasing age contributes to the overall decreased enhancement of the epiphyseal cartilage (18,27,28). Cartilage-sensitive MR imaging sequences such as gradient-recalled-echo (GRE) imaging and spoiled gradient-recalled-echo (SPGR) imaging facilitate excellent contrast between the often bright cartilage and the dark bone and are excellent for identifying areas of growth plate closure (29,30) (Fig 7b). The main obstacles to using MR imaging more routinely in children are the possible need for sedation, limited immediate availability, and higher cost.

Direct Growth Plate Disturbances

Insult to the growth plate can be direct (affecting the growth plate), indirect (affecting the epiphysis and metaphysis), or both (Fig 3). The following section will focus on the pathophysiology and deformities that can result from fractures involving the growth plate, which are the most common cause of direct growth plate disturbance.

Growth Plate Fractures

Eighteen percent of all fractures in children involve the growth plate (31). In skeletally immature children, fractures often are centered at or extend into the primary growth plate, which is a specific site of weakness and approximately two to five times weaker than the surrounding soft-tissue structures (32,33). These fractures are more common in boys, occur more frequently in the upper extremities (31,34), and are more prevalent during adolescent growth spurts; they are 5% more common in persons 13–17 years of age than in those 5–12 years of age (33). The greater prevalence of these fractures during growth spurts is postulated to be due to a combination of longitudinal growth outpacing bone mineralization, resulting in temporarily more fragile bone (35); the increased ability of

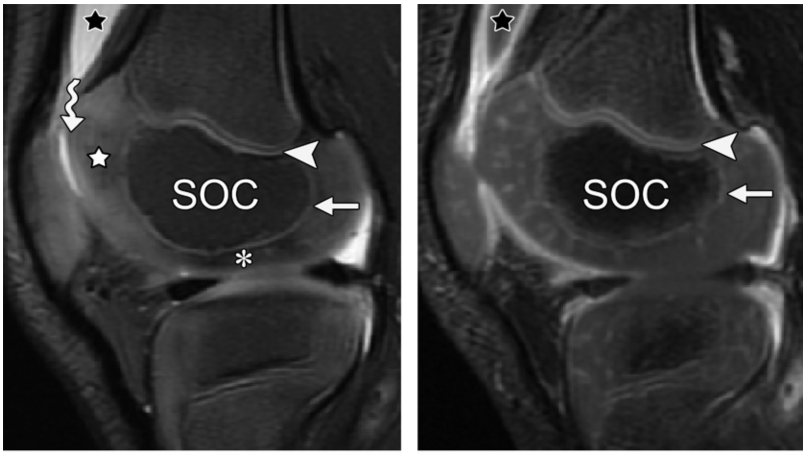

a. b.

Figure 6. Normal differences in hyaline cartilage signal intensity in the knee of a 3-year-old girl. **(a)** Sagittal T2-weighted fat-saturated MR image shows that the articular cartilage (wavy arrow) and growth plate cartilages (comprising primary growth plate [arrowhead] and acrophyseal [straight arrow] cartilages) are relatively more hyperintense than the epiphyseal cartilage (☆) owing to greater organization of the collagen fibrils (in articular cartilage) and water molecules that are less tightly bound to macromolecules (in primary growth plate and acrophyseal cartilages). Note the focal decrease in signal intensity in the weight-bearing portion of the cartilage (*), which is related to the local displacement of water and often observed after the onset of walking (2). **(b)** Sagittal T1-weighted fat-saturated MR image obtained 2 minutes after contrast material administration shows the growth plate cartilages (arrow and arrowhead) with homogeneous avid enhancement, as compared with the epiphyseal cartilage, in which only the vascular channels are enhanced. The canalicular and cartilaginous phases of progressive epiphyseal enhancement (not shown) occur 5–10 minutes after the contrast material administration. The trilaminar appearance of the growth plate reflects a combination of the bright cartilaginous portion of the growth plate, dark ZPC, and bright primary spongiosa. A joint effusion (★ in **a** and **b**) with surrounding enhancing synovitis is present secondary to this patient's underlying juvenile idiopathic arthritis.

this age group to generate force; and involution of the perichondral sleeve that stabilizes the chondro-osseous junction (36).

With the Salter-Harris fracture classification system, these physeal fractures are subdivided on the basis of their radiographic appearance and/or causal mechanism (9). Although additional types and variants have been proposed, the original five fracture types remain the most widely utilized (36). Type I fractures, accounting for 6.0%–8.5% of growth plate fractures, are transverse cleavages through the growth plate. If the fracture extends into the ZPC and is of sufficient size to be radiographically apparent, then a lamellar fragment is observed. Type II fractures, accounting for 73%–75% of growth plate fractures, involve the metaphysis; type III fractures, accounting for 6.5%–8.0% of growth plate fractures, involve the epiphysis; and type IV fractures, accounting for 10%–12% of growth plate fractures, involve the metaphysis and epiphysis (9). For type IV Salter-Harris fractures, surgical restoration of the joint surface realignment is often required, and these injuries are more worrisome owing to the potential for transphyseal vascularity, which facilitates the recruitment of osteoprogenitor cells and thus leads to subsequent bridge formation (37–39) (Fig 4). Interestingly, in contrast to the commonly held belief that the growth plate fracture cleavage planes are typically limited to the dying chondrocytes of the hypertrophic zone (9,40,41), Jaramillo and colleagues (8) found that up to 64% of these fractures also involve the reserve and proliferative zones. Relatively rare type V fractures account for less than 1% of growth plate fractures; this category is reserved for fractures involving longitudinal compression of the reserve zone of the growth plate. However, this injury can be diagnosed only retrospectively, after the development of a structural deformity resulting from premature growth plate closure (9,42,43). Controversies exist because these deformities are nonspecific and more likely to result from an electrical injury, frostbite, or irradiation (44).

Although the Salter-Harris classification system is excellent for characterizing fractures, it lacks prognostic value. For example, in the distal tibia, the incidence of premature growth plate closures following type I and type II Salter-Harris fractures is 36%, which is not substantially different from the 38% incidence of these closures following type III and type IV Salter-Harris fractures (45). Rather, the anatomic location (9) and/or growth

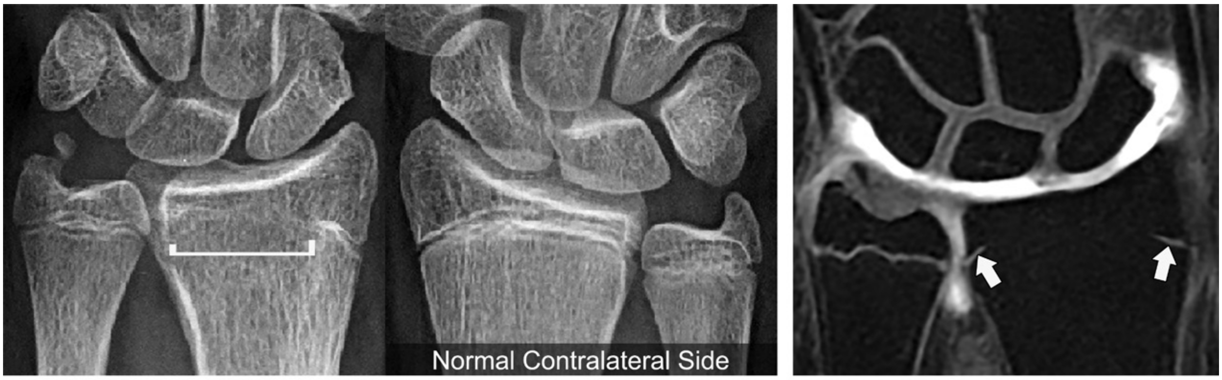

a. b.

Figure 7. Growth plate closure in a 13-year-old girl 1 year after a type II Salter-Harris fracture. **(a)** Left: Posteroanterior radiograph of the injured left wrist shows central closure (bracket) of the primary growth plate. The ulnar variance remains neutral. An ulnar styloid fracture also is present. Right: Posteroanterior radiograph of the normal right wrist is shown for comparison. **(b)** Findings on a coronal GRE cartilage-sensitive MR arthrogram of the left wrist confirm the presence of a large area of central growth plate closure with normal peripheral growth plate cartilage (arrows).

plate contour seems to be more predictive of the prognosis. For example, fractures through the uniplanar, relatively smooth growth plate of the distal radius are common but rarely cause growth arrest (31). Conversely, fractures through the multiplanar undulating growth plates of the distal femur and distal tibia are uncommon but lead to growth arrest in 40% of distal femoral fractures and 20% of distal tibial fractures (46). This is because the fracture cleavage plane for these undulating growth plates typically extends into the adjacent epiphysis and metaphysis and is therefore more likely to lead to transphyseal vascularity, a precursor to bridge formation (37).

Radiography remains the preferred initial imaging modality of choice for the detection of acute fractures, subacute healing response, and subsequent growth disturbances (9). Radiographs are readily available, do not involve patient sedation, and enable quick and serial assessment. Rarely, an acute nondisplaced or crush injury isolated to the radiolucent growth plate can be subtle or completely radiographically occult and diagnosed only retrospectively on the basis of subsequent healing response and/or resulting growth disturbance. The awareness of this radiographic limitation has led to the use of CT, scintigraphy, and MR imaging.

CT provides excellent bone detail, which is helpful for the detection of tiny osseous bridges and surgical planning. Following acute fractures, CT can help to determine precise intra-articular alignment and identify small fracture fragments (9). The main disadvantages of CT are the radiation exposure, inability to evaluate the cartilaginous growth plate and epiphysis, and inability to assess osteochondral perfusion. Radionuclide studies are rarely used owing to the requirement for radiation exposure, lack of anatomic spatial resolution, and potential requirement for sedation. MR imaging is used occasionally in the acute setting to assess equivocal cases. Acute fractures through the growth plate can cause high signal intensity on fluid-sensitive MR images (47,48), loss of the normal bright growth plate signal on GRE MR images, and a cleft of nonenhancement following contrast material administration (8). MR imaging can be used to concurrently evaluate the fractured area for possible vascular compromise, periosteal disruption, and surrounding soft-tissue injury. The results of previous studies (49–51) have not led to a consensus regarding whether MR imaging–based reclassification of growth plate fractures alters clinical management and prognoses. Therefore, MR imaging currently should be reserved for assessment of suspected occult (39,51,52) and complex fractures (49).

Soft-Tissue Physeal Interposition

The interposition of soft tissue into the growth plate following a fracture is uncommon; however, it is important to identify because open surgical reduction will be required if it is found. The trapped soft tissue is most commonly a torn piece of metaphyseal periosteum; less common entities include a ligament, tendon, muscle, or neurovascular bundle. Soft-tissue interposition should be suspected when postreduction radiographs show persistent growth plate widening of more than 3 mm. In these situations, the incidence of premature physeal closure increases to 60%, as opposed to an incidence of 17% in cases without growth plate widening (45). There is a higher rate of bridge formation for the interposed periosteum because of its natural propensity to form bone (53,54). At all MR imaging pulse sequences, the entrapped periosteum appears as a well-defined

Figure 8. Periosteal interposition in a 14-year-old boy after a fracture. **(a)** Lateral ankle radiograph obtained after the reduction and casting of a type II Salter-Harris fracture (arrowheads) shows persistent anterior growth plate widening (double-headed arrow) measuring 3.4 mm. **(b)** Sagittal T1-weighted MR image confirms the presence of the fracture (arrowhead) and intraphyseal displacement of a torn low-signal-intensity metaphyseal periosteum (wavy arrow). **(c)** Left: Sagittal CT image obtained 1 year later shows an osseous bridge (bracket), with tethering of the growth recovery line (arrow) due to asymmetrically slowed longitudinal growth of the anterior tibia relative to the posterior tibia. Right: Sagittal CT image of the normal contralateral side is shown for comparison.

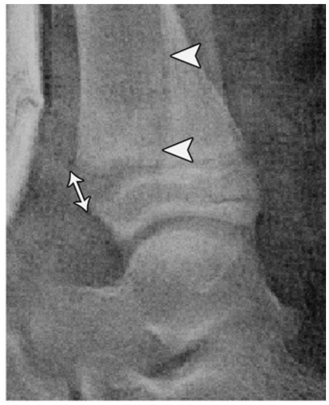

a.

b.

c.

band of low signal intensity extending from the bone surface into the growth plate (Fig 8).

Slipped Capital Femoral Epiphysis

A slipped capital femoral epiphysis is the most common cause of hip disease in obese adolescents (55,56), with an incidence of two per 100 000 children. It is 2.5-fold more common in boys and can be bilateral in up to 37% of cases (56). Although the exact cause of a slipped capital femoral epiphysis is unknown, leading hypotheses favor a combination of mechanical stress and hormonal imbalance (57). Histopathologic analyses reveal growth plate widening, architectural distortion with diminished cellularity, premature apoptosis, and an abnormal distribution of matrix proteins (58–61). It is uncertain whether these findings reflect a healing response to prior subclinical microslips (57) or a preexisting diseased growth plate that is predisposed to the acute slip (62). The fracture plane often involves the proliferative and hypertrophic zones (58). Although growth plate injury predominates, concurrent dysfunction of endochondral ossification (reflecting metaphyseal injury) is often observed, with chondrocytes extending into the metaphysis.

Radiographic findings often include growth plate widening and metaphyseal irregularity. Progressive posterior or posteromedial displacement and rotation of the femoral head relative to the neck produce an apparent diminished height of the femoral head on anteroposterior radiographs. The tenuous blood supply to the intracapsular femoral head epiphysis may be kinked or frankly disrupted during the slip and/or tamponaded owing to the increased intracapsular pressure. In up to 21% of cases, this results in epiphyseal osteonecrosis, which can lead to further indirect injury of the growth plate (36,63). MR imaging is increasingly being used to evaluate slipped capital femoral epiphyses and identify cases of preslip. MR imaging can be used to confirm growth plate widening, which is best depicted on T1-weighted images; assess possible associated bone marrow edema and joint effusion, which are best depicted on fluid-sensitive images (56); and evaluate femoral head perfusion on contrast material–enhanced images (64). Cases of preslip are by definition radiographically occult, but MR images can show subtle growth plate widening with possible associated bone marrow edema and joint effusion (56,64). If left untreated, preslip will progress to

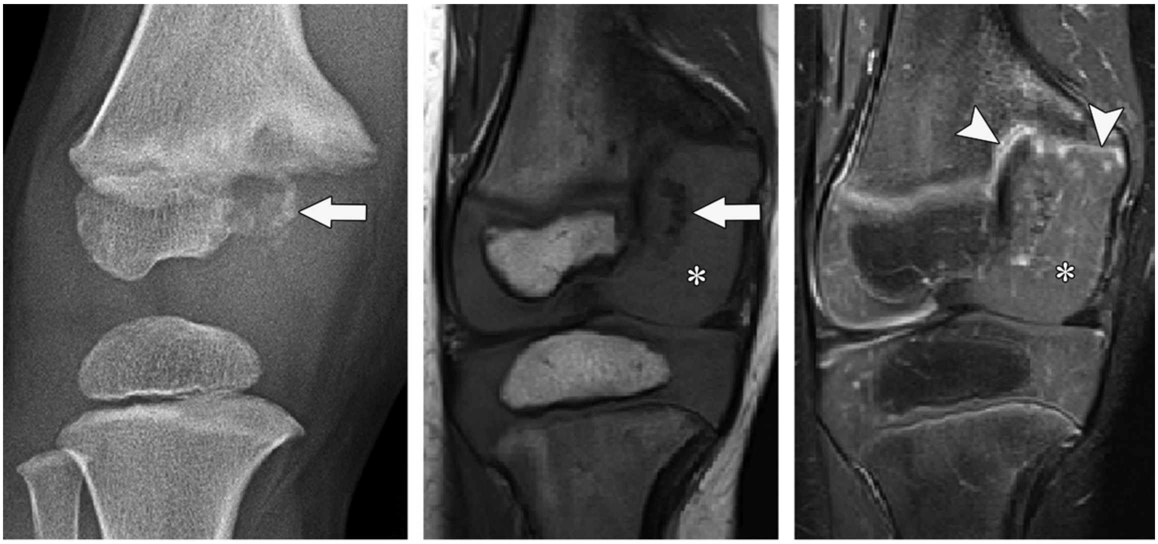

a. b. c.

Figure 9. Right knee deformity in a 2-year-old adopted boy. Anteroposterior radiograph **(a)** and coronal T1-weighted nonenhanced **(b)** and contrast-enhanced fat-saturated **(c)** MR images show a small medial femoral SOC (arrow in **a** and **b**) with fragmentation and an absence of yellow marrow signal. The slower longitudinal growth across the medial distal femur results in apparent proximal displacement of the underlying growth plate (arrowheads in **c**), which remains open. Note the abundant nonossified medial epiphyseal cartilage (* in **b** and **c**).

a slipped capital femoral epiphysis (65). The goal in providing treatment is to stabilize the femoral head; however, currently, there is no consensus regarding the optimal technique, timing of intervention (64,66), and whether fracture reduction protects against or further induces osteonecrosis (66). The rate of posttreatment osteonecrosis is widely variable and depends on the preoperative hip stability and surgical approach (63).

Indirect Growth Plate Disturbance Involving the Epiphysis

The growth plate is avascular and relies on an intact blood supply from the adjacent epiphysis and metaphysis to maintain chondrocyte proliferation and ensure apoptosis. Epiphyseal osteonecrosis can cause indirect growth plate dysfunction and thus lead to a combination of characteristic findings with variable degrees of severity, such as an abnormal SOC, slowed longitudinal growth, and/or bridge formation (47) (Fig 9). Epiphyseal osteonecrosis can be idiopathic or result from a variety of secondary causes.

Legg-Calvé-Perthes Disease

Legg-Calvé-Perthes disease is an idiopathic self-limited osteonecrosis of the proximal femoral epiphysis that commonly occurs during late childhood, in children 5–10 years of age, with an incidence of 0.2–29.0 cases per 100 000 children. It is more common in white children and boys (fourfold), and it can be bilateral in up to 10% of cases (19). The underlying pathophysiologic mechanism is postulated to involve disruption of the femoral head blood supply in genetically susceptible individuals following subclinical trauma or mechanical loading (67). Between 3 and 8 years of age, only the medial circumflex artery supplies the proximal femoral epiphysis. This is in contrast to a dual arterial supply before 3 years of age with the addition of the lateral circumflex artery and after 8–10 years of age with the addition of the artery of the ligamentum teres (68). Epiphyseal infarction often injures the primary growth plate, which consequently exhibits disorganization with uneven staining of the cartilage matrix (69), reduced collagen and proteoglycan granules, and increased large lipid inclusions at histopathologic analysis (70). Although epiphyseal injury predominates, histopathologic examinations commonly reveal additional metaphyseal involvement, with cysts and chondrocytes within the metaphysis (69,71).

The spectrum of deformity is based on the overall extent of injury. The proximal femur has a unique L-shaped bifid growth plate with medial, vertex, and lateral portions. The medial portion normally grows twice as fast relative to the lateral portion and is the main contributor to the formation of the femoral neck. The lateral portion is mainly responsible for the growth of the greater trochanter. The vertex, located between the medial and lateral portions, is the most active area of growth and therefore also the most prone to ischemia (72). Medial growth arrest causes a

Figure 10. Legg-Calvé-Perthes disease in a 2-year-old boy. **(a, b)** Anteroposterior pelvic radiograph **(a)** and T1-weighted nonenhanced (left) and contrast-enhanced fat-saturated (right) MR images **(b)** show early SOC fragmentation (arrows) and a lack of left femoral head enhancement (arrowhead in **b**) after contrast material administration. **(c)** Anteroposterior radiograph obtained 5 years later shows a flattened left femoral head with lateral uncovering by the acetabulum, as well as a short and broadened neck. The central metaphyseal bone peak (wavy arrow) and diffuse growth plate narrowing and irregularity raise concern for an impending premature growth plate closure. This patient is at risk for future joint incongruity, labral degeneration and tearing, coxa vara deformity, limb length discrepancy, and early osteoarthritis.

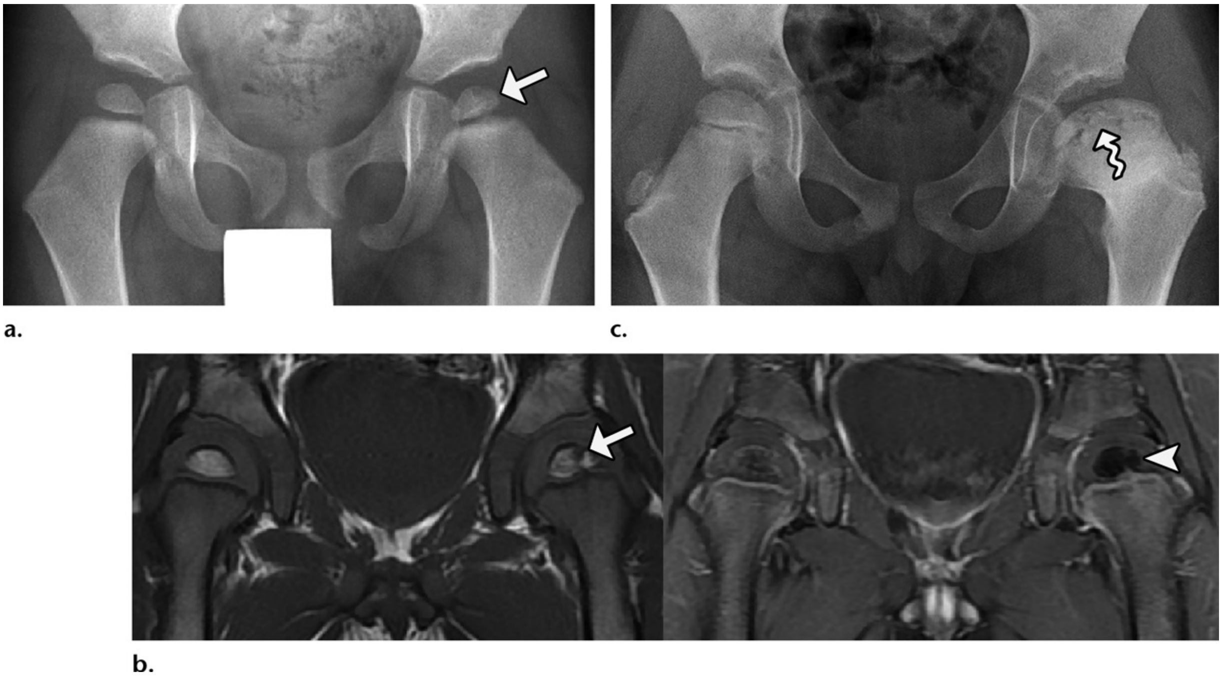

short, wide femoral neck and coxa vara deformity, whereas vertex growth arrest causes a coxa valga deformity. True lateral growth arrest is uncommon (3,72). The resulting deformity often reflects a combination of these extremes. Overall, premature growth plate closure has an incidence of 12.8%, with the growth plate closing, on average, 2–5 years earlier than the contralateral normal hip (73). The closure often begins at a metaphyseal peak, projecting toward the epiphysis, which then transforms into an osseous bridge during early adolescence and is followed by progressive closure of the remainder of the growth plate (Fig 10).

During the acute phase of disease, radiographs often show normal findings (69). MR images show bone marrow edema and decreased or absent enhancement in the proximal femoral epiphysis, as well as joint effusion (74). Since the anterior femoral head is more often involved, sagittal images most accurately depict the full extent of involvement (74). Studies have shown that MR imaging can be used to detect early growth plate involvement (75), and the development of transphyseal enhancement is a risk factor for bridge formation (76). Poor prognostic indicators include older patient age (>7 years) at disease onset (77), severe head deformity (78), lateral pillar collapse (67), growth plate involvement (79,80), and metaphyseal lesions (71).

The radiographic appearance of Legg-Calvé-Perthes disease during the subacute and reparative phases can be divided into four stages: avascular necrosis, fragmentation, regeneration, and healed (77,81). Untreated end-stage disease can cause an enlarged and deformed femoral head (coxa magna or coxa irregularis), relative trochanteric overgrowth, femoroacetabular impingement, and leg length discrepancy (77), with more than half of affected individuals developing disabling osteoarthritis by the 6th decade of life (67). Therefore, the goals in providing treatment are to contain the femoral head within the acetabulum and preserve joint congruity during the early fragmentation stage with use of bracing, abduction casts, and femoral and/or pelvic osteotomy (82).

Hyperabduction Osteonecrosis

Osteonecrosis can occur as a complication of open or closed hip reduction in children who have developmental dysplasia of the hip, with a prevalence of 6%–47% (83). It is thought to be caused by hyperabduction and increased intracapsular pressure. Hyperabduction can cause anterior ischemia due to vascular obstruction and posterolateral ischemia due to compression of the epiphyseal vascular channels against the posterior acetabular rim (84). Increased intracapsular pressure is often attributed to venous congestion (85) and/or a dysplastic anatomy

Figure 11. Left developmental dysplasia of the hip in a 10-month-old boy. **(a)** Intraoperative arthrogram shows a hypoplastic acetabulum (wavy arrow) with blunting of its superolateral rim and a superolaterally dislocated left femoral head (☆). **(b)** Axial contrast-enhanced T1-weighted fat-saturated MR image obtained after a successful reduction procedure shows a lack of enhancement of the left femoral epiphysis, including the SOC (arrowhead). Note the normal right epiphysis, with enhancement of the SOC (straight arrow) and cartilage vascular channels (curved arrow). **(c)** Anteroposterior pelvic radiograph obtained 9 months later shows interval growth of the right SOC (arrow), an absent left SOC, and a relatively narrow medial left femoral growth plate (short double-headed arrow), with asymmetrically blunted medial longitudinal growth (short bracket), compared with the medial right femoral growth plate (long double-headed arrow) and longitudinal growth (long bracket). These findings are in keeping with primary epiphyseal osteonecrosis that involves the medial growth plate. This patient is at risk for proximal migration of the greater trochanter, coxa vara deformity, and limb length discrepancy.

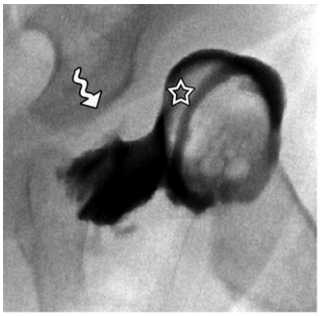

a.

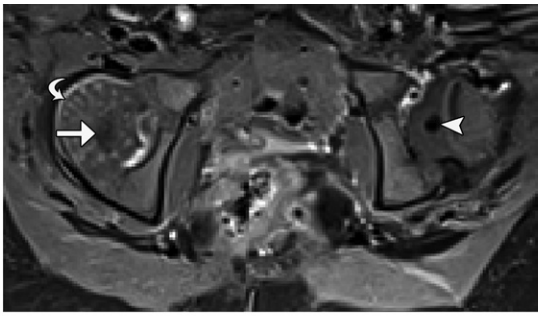

b.

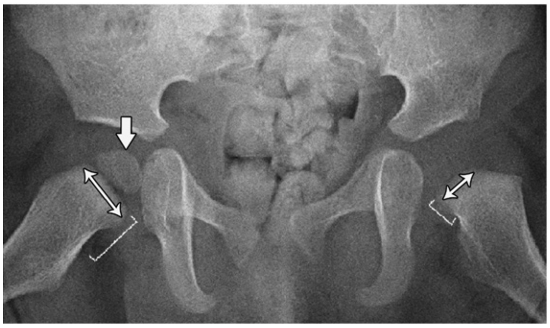

c.

(86,87). Premature growth plate closure occurs in up to 60% of cases with epiphyseal ischemia (88). As with Legg-Calvé-Perthes disease, with hyperabduction osteonecrosis, the medial and vertex portions of the proximal femoral growth plate are most often involved and the resulting growth deformity is based on the predominant site of injury (72) (Fig 11).

Posttraumatic Osteonecrosis

Fishtail deformity, an example of posttraumatic osteonecrosis, is the result of a rare delayed complication of distal humerus fractures, which may be supracondylar or condylar, displaced or nondisplaced, or with or without internal fixation (89–91). Patients typically present with a limited range of motion, pain, and cubitus valgus deformity during late childhood or early adolescence. Their delayed presentation—on average 5 years after the initial traumatic event (92)—is partially attributed to the late radiographic appearance of the trochlear SOC, which typically occurs when the child is 7–10 years of age (91). Proposed causes include osteonecrosis and/or premature growth plate closure (90). The lateral trochlea is a watershed area that is prone to vascular disturbances. It is located between the shaft, which is supplied by the nutrient artery, and the medial and lateral columns of the distal humerus, which are supplied by anterior and posterior segmental vessels (93).

Stereotypical imaging findings include a focal concavity of the central aspect of the distal humerus, which corresponds to a hypoplastic or absent lateral trochlear ossification center, with relatively normal growth of the remainder of the distal humerus; this process causes a “fishtail,” or inverted V configuration (Fig 12). Comparison of radiographs of the symptomatic and asymptomatic elbows is recommended, because the trochlear SOC is often multicentric, irregular, and granular, and, thus, there is wide variation in its normal appearances (89). The fishtail configuration can mimic the morphology of Hagemann disease, which is a rare self-limited idiopathic osteonecrosis of the trochlea; to date, there are only eight reported cases where more than half of these cases report mild antecedent injury. It is uncertain whether Hagemann disease is an entirely separate disease or represents a milder form of fishtail deformity (89).

MR imaging can be used to delineate the underlying growth plate, evaluate the nonossified trochlear anatomy, detect early osteoarticular findings, and identify the development of osteochondritis dissecans of the capitulum due to increased lateral column loading (91). Symptomatic patients with intra-articular bodies, proximal migration of the forearm, and/or radial

a. b. c.

Figure 12. Fishtail deformity in a 15-year-old girl. **(a)** Anteroposterior radiograph shows a displaced supracondylar fracture that was treated without immediate complications. **(b, c)** Anteroposterior radiograph **(b)** and corresponding coronal proton-density–weighted fat-saturated MR image **(c)** obtained 5 years later show a central concavity of the distal humerus (bracket in **b**) secondary to an almost completely absent lateral trochlea; these findings are theorized to be the sequelae of posttraumatic osteonecrosis of this watershed area. The medial trochlea (arrow) is present. Note the degenerative subchondral cysts (arrowheads in **c**) that developed as a result of chronic altered biomechanics.

head subluxation may require surgical restoration of the joint congruity with arthroplasty, débridement, epiphysiodesis of the adjacent normal growth plate, and/or ulnar nerve transposition (89,91,92).

Tibia Vara

Blount disease, or tibia vara, is a relatively uncommon disorder that causes a characteristic abnormal growth of the medial or posteromedial proximal tibia. The early-onset type, which occurs in children 3 years of age or younger, is more likely to have bilateral involvement, while the later-onset type, which includes a juvenile form that occurs between 4 and 10 years of age and an adolescent form that occurs after 10 years of age, is more likely to affect males and African-American children (94). It is uncertain whether these two types represent a spectrum of the same disease process or are two distinct entities that manifest with similar features (94). The exact causal mechanism remains unclear, with leading theories favoring a combination of genetic predisposition and chronic stress (13,95). The abundance of nonossified epiphyseal cartilage makes MR imaging the ideal modality for studying this entity. Findings include hypertrophy of the nonossified epiphyseal cartilage, delayed ossification and fragmentation of the medial SOC, metaphyseal displacement of the growth plate, and variable degrees of medial meniscus hypertrophy (Fig 13). Initial study results (96) suggest that MR imaging is more accurate than CT for detection of a transphyseal bridge. Surgical treatment involves varus correction osteotomy and, if a bridge is present, bridge resection (95).

Osteomyelitis

Osteomyelitis has an annual incidence of two to 13 cases per 100 000 children in developed countries, with 33% of cases occurring in children during their first 2 years of life (21). The growth plate injury can be direct or indirect, depending on the child's stage of development and the infectious organism. In infants, transphyseal vascular channels allow the spread of hematogenous infection from the metaphysis into the epiphysis (14). Epiphyseal infection, if severe enough, can cause epiphyseal ischemia that may indirectly injure the growth plate (97) (Fig 14). After a child is 12–18 months of age, the involution of transphyseal vessels leads to an increased incidence of metaphyseal osteomyelitis as a result of local vascular stasis within the terminal arterial loops (21). In contrast to the classic belief that the avascular growth plate serves as a barrier to the transphyseal spread of infection, relatively recent data indicate that up to 81% of patients 2–16 years of age with pyogenic infection have MR imaging findings of transphyseal spread that has been postulated to represent direct injury of the underlying growth plate (98). However, the long-term clinical implication of this imaging finding has not yet been studied.

Meningococcemia occurs in 10%–20% of individuals who have diffuse meningococcal infection. The meningococcal endotoxin triggers diffuse vasculitis, thrombosis, and hemorrhage (99), which lead to multifocal ischemia (100). Skeletal deformities result from a combination of osteonecrosis and osteoarticular infection. In infants and young children who have an abundance of radiolucent cartilage and are often unable to localize their

a. b. c.

Figure 13. Tibia vara in a 10-year-old girl. **(a)** Anteroposterior radiograph of the left knee shows a characteristic Blount deformity of the medial proximal tibia, which includes abnormal metaphyseal "beaking" from metaphyseal downsloping, distal displacement of the growth plate (arrowhead), and fragmentation of the diminutive medial portion of the tibial SOC. **(b, c)** Findings on coronal proton-density–weighted MR images without **(b)** and with **(c)** fat saturation confirm displacement of the medial growth plate (curved arrow in **c**) with a small bridge (straight arrows). Note the normal lateral growth plate (arrowhead in **c**) and abundance of medial nonossified epiphyseal cartilage (∗). For a favorable surgical outcome, resection of the bridge—if one is present—performed at the time of corrective osteotomy is required.

Figure 14. Growth plate injury in a 2-year-old girl with a history of neonatal methicillin-resistant *Staphylococcus aureus*–related sepsis. Anteroposterior pelvic radiograph shows an asymmetrically smaller left femoral SOC (arrowhead), bilateral metaphyseal sclerosis, and relatively blunted growth of the vertex of the proximal femoral growth plates (arrows). These findings are probably the result of regional infectious and/or ischemic insults to the lateral epiphyses that also affected the adjacent growth plates. The relatively slower differential growth across the injured vertex places this child at risk for future coxa valga deformities and lateral femoral head uncovering.

symptoms, it is notoriously difficult to detect the acute insults on screening radiographs. Rather, the growth disturbance becomes apparent years later, with findings of an abnormal SOC, angulation, and limb shortening (101,102) (Fig 15). Therefore, follow-up with annual radiography until skeletal maturation is recommended for these patients to ensure the detection of early signs of growth disturbance (102,103). The surgical correction is based on the patient's age and involves a combination of guided growth with selective epiphysiodesis, wedge osteotomy, or both.

Indirect Growth Plate Disturbance Involving the Metaphysis

In contrast to the nourishing epiphyseal vessels, the metaphyseal vessels do not supply blood to the growth plate. Instead, the main function of the metaphyseal vessels is to trigger chondrocyte apoptosis, matrix mineralization, and endochondral ossification (15). Therefore, metaphyseal vascular compromise leads to prolonged survival of hypertrophic chondrocytes, producing lengthening of the chondrocyte columns, which can appear as growth plate widening (104). Laor and colleagues (15) found two distinct patterns of chondrocyte extension into the metaphysis, which often correlate with the mechanism of injury: a focal "tongue" of persistent cartilage from focal injury versus a "broad band" from repetitive microtrauma. They also noted that the overall prognosis is better for patients with repetitive microtrauma, postulated to reflect less complete vascular disruption (Fig 16). The indirect growth plate injuries that result from single or limited insults to the metaphysis, such as metaphyseal fracture and treatment-related osteonecrosis, as well as those from repetitive insults to the metaphysis, such as overuse and recurrent fractures, are reviewed in the following sections. Rickets, hypophosphatasia, and mucolipidosis, which can cause apparent growth plate widening from failed mineralization and systemic metabolic imbalances, are beyond the scope of this review.

Metaphyseal Fracture

Although metaphyseal injuries are more commonly encountered as part of type II and type IV Salter-Harris fractures, their pathophysiology and effect on the growth plate are better studied in children who have "bucket-handle" or "corner" fractures that are typically associated with nonaccidental trauma. The cleavage plane of these

Figure 15. Growth disturbance in a 5-year-old boy with a history of meningococcemia. **(a, b)** Anteroposterior bilateral ankle radiographs **(a)** and coronal right ankle GRE MR image **(b)** show an osseous bridge (brackets) involving the right medial distal tibia. In **a,** the normal appearance of the left ankle is shown for comparison. The relatively normal appearance and function of the adjacent right lateral distal tibial growth plate (arrowhead) led to differential longitudinal growth and resultant varus alignment. **(c)** Axial reformatted maximum intensity projection MR image obtained at the level of the growth plate is used with the following formula to estimate the percentage of the growth plate that is replaced by a bridge (arrowheads): $(a_b/a_g) \times 100$, where a_b is the area of the bridge and a_g is the area of the entire growth plate. In this case, the bridge occupies less than 50% of the growth plate, making this patient a candidate for bridge resection.

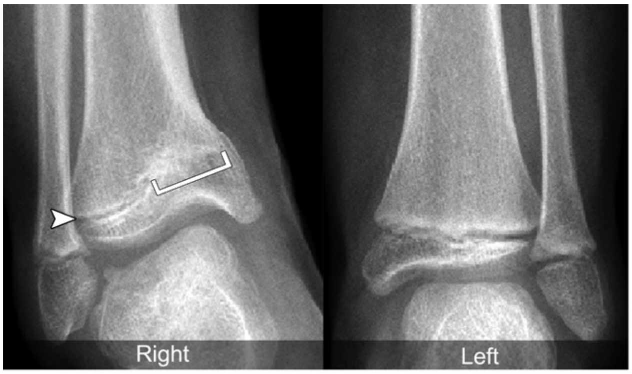

a.

b.

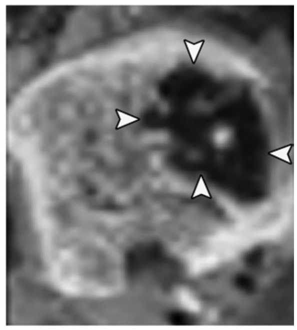

c.

fractures is centered within the primary spongiosa, causing focal disruption of normal endochondral ossification (105). In animal models, increased signal intensity on fluid-sensitive images and widening of the growth plate can be detected as early as 24 hours after the injury. The progressive widening of the growth plate occurs in a linear fashion during the first 2 weeks (47), which, theoretically, can be used to estimate the time between the initial injury and the imaging study (105).

Treatment-related Osteonecrosis

Bone infarction occurs in 6.5%–15.0% of patients with acute lymphoblastic leukemia, which is the most prevalent subtype of acute leukemia in children. It is a common complication of chemotherapeutic treatment, and patients often present with nonspecific bone pain (21). If the osteonecrosis involves the juxtaphyseal metaphysis, then focal disruption of endochondral ossification may occur and lead to focal growth plate widening (Fig 17). If the focus of persistent metaphyseal chondrocytes abuts a growth recovery line and the margin of an infarct, then this suggests that the vascular insult, often from chemotherapy, led to both findings and the height of the chondrocyte column corresponds to the time between insult and imaging (15,106).

Overuse Injury

Sports-related growth plate injuries can be acute or chronic. Acute injuries occur with a variety of sports activities, and the overall prevalence ranges from 1% to 12%, with 0%–75% of cases resulting in growth disturbance (35). *Chronic microtrauma* is defined as repetitive submaximal stress that exceeds the injury repair rate (35), and cases of these injuries are increasing because of growing participation in sports, sports subspecialization, and the increasing physical intensity of sports training (107). The spectrum of overuse osseous injuries includes growth plate stress underlying epiphyses and apophyses, diaphyseal stress reaction and fractures, and osteochondral injuries (107). Common sites of stress are the distal radius and ulna in gymnasts; distal femur, proximal tibia, and distal fibula in runners; and proximal and distal humerus in baseball pitchers (9). Patients often present with chronic pain that is localized to the level of the growth plate, worsens during training, and is initially relieved with rest. Radiographs show widening of the growth plate, an indistinct ZPC, and subtle irregularity and sclerosis of the metaphysis (9). With gymnast wrist, these findings are commonly bilateral and involve the entirety or volar aspect of the distal radial physis, with up to 20% of radiographs also showing concurrent findings within the distal ulna. MR images show periphyseal edema and growth plate widening (9). Although the metaphyseal abnormality predomi-

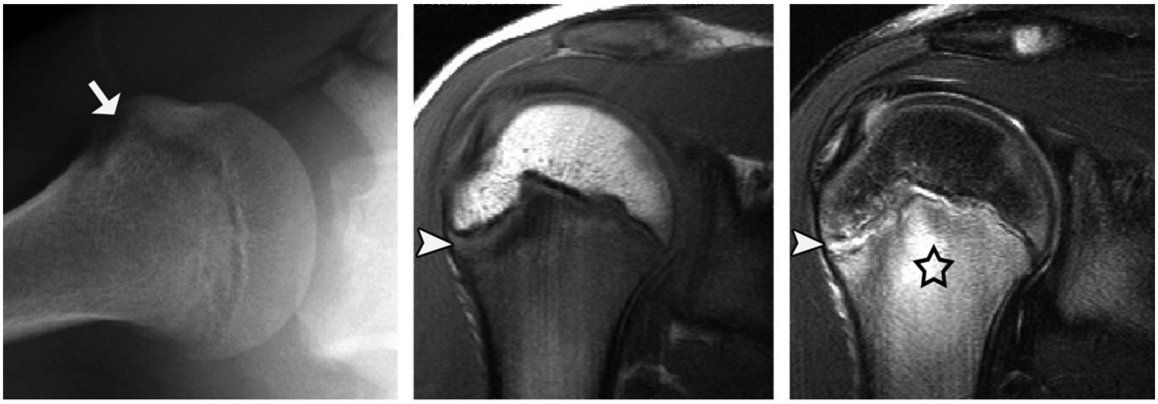

a. b. c.

Figure 16. Growth plate stress injury in a 14-year-old boy, a baseball pitcher, with shoulder pain. **(a)** Axillary radiograph shows subtle widening of the anterior humeral growth plate (arrow) and an indistinct adjacent ZPC. **(b, c)** Findings on oblique coronal T1-weighted **(b)** and T2-weighted fat-saturated **(c)** MR images confirm the presence of a physeal injury (arrowheads) with adjacent reactive bone marrow edema (☆). This location and appearance are typical of chronic growth plate stress injury of the humerus in young pitchers, better known as "little leaguer shoulder."

a. b. c.

Figure 17. Metaphyseal osteonecrosis in a 5-year-old girl who had ankle pain following chemotherapy for acute lymphoblastic leukemia. Oblique left ankle radiograph **(a)** and corresponding coronal proton-density–weighted fat-saturated **(b)** and sagittal T1-weighted **(c)** MR images show a growth recovery line (arrowheads) that parallels the underlying growth plate (curved arrow in **a** and **b**). Multifocal treatment-related osteonecrosis (straight arrows in **b** and **c**) is present. A thickened band of nonossified growth plate cartilage (*) persists within the metaphysis owing to focal disruption of endochondral ossification as a consequence of the adjacent metaphyseal osteonecrosis.

nates, there is probably an associated injury of the growth plate and epiphysis, which explains the occasional cases of permanent growth arrest (108) and long-term deformity (109–111). If an overuse osseous injury is diagnosed early, conservative treatment involves time off from sports and bracing, which enable the reconstitution of metaphyseal perfusion. Healing occurs with centripetal ossification of the metaphyseal cartilage rests, which leads to normalization of the growth plate and reconstitution of the ZPC (15,47) (Fig 18).

Insensitivity to Pain

Ten percent to 30% of individuals who have myelomeningocele will sustain fractures, with 10% of these cases involving the growth plate (9). The combination of sensory deficiency, musculoligamentous laxity, and a demineralized state predisposes the lower extremities of these individuals to chronic stress resulting in refractures and delayed healing (112). Imaging findings can include growth plate widening, metaphyseal irregularity, and abundant surrounding callous

a. b.

Figure 18. Overuse osseous injury in a 13-year-old female gymnast with wrist pain. **(a)** Posteroanterior radiograph shows growth plate widening (arrowheads) and metaphyseal irregularity of the distal radius and (to a lesser extent) of the ulna due to repetitive microtrauma. These findings are bilateral and symmetric. The contralateral side is not shown. **(b)** Posteroanterior radiograph obtained 9 months later, after activity restriction, shows resolved growth plate widening, a reconstituted ZPC (wavy arrow), and no premature growth plate closure.

formation due to continued motion at the fracture site (113). Although the pain and swelling mimic the clinical manifestations of osteomyelitis, the lack of infectious symptoms, abundance of callous formation and sclerosis, and response to immobilization favor a healing fracture (Fig 19). In equivocal cases, bone biopsy may be required to render a definitive diagnosis. Biopsy will reveal a thickened and disorganized hypertrophic zone and an additional vascularized zone of fibrous tissue adjacent to the metaphysis, (9). Treatment is focused on prolonged immobilization with periodic radiologic monitoring. Occasionally, an isolated widening of the growth plate that normalizes with activity limitation and orthoses is observed. This finding has been postulated to represent a "prefracture" state that is more susceptible to injury; this results from the temporary disruption or delay in mineralization of the ZPC and osteogenesis (114).

Although we have reviewed direct and indirect growth plate insults as separate entities (Fig 3), it is important to remember that most insults are not limited to one component of the growth plate complex. Rather, they often affect multiple components and cause a combination of findings.

Imaging and Treatment of Growth Disturbance

Focal bridges and diffuse premature growth plate closure are the end results of permanent growth plate injuries. Up to 70% of bridges are posttraumatic (46,115) and can occur after all types of Salter-Harris fractures (36,43,45,116). The main prognostic factors of bridge formation include type of fracture, severity of injury, number of attempted reductions, and method of treatment (39). Bridge management is individualized and based on a combination of patient factors—such as anticipated growth, anatomic location, and deformity characteristics—and imaging findings (38). Therefore, accurate depiction of the location and extent of growth plate involvement will ensure the selection of the most appropriate treatment.

CT traditionally has been used to estimate the size of a bridge. On CT images, an osseous bridge appears as a focal loss of normal growth plate hypoattenuation with or without adjacent reactive sclerosis (Fig 8c). However, with CT, fibrous bridges can be missed and neither the cartilage nor the soft tissue can be fully assessed (38); this modality is also less accurate when applied to multiplanar and tortuous growth plates (117). Therefore, MR imaging is being used increasingly (39). Thin-section (<1-mm) three-dimensional fat-saturated cartilage-sensitive MR imaging sequences such as GRE imaging with low (~20°) flip angles provide excellent contrast between bright cartilage and dark bone (29,30) and enable multiplanar reformations (118) that facilitate calculation of the bridge size (Fig 15c) (29). Large bridges with fatty marrow are best depicted on T1-weighted MR images, whereas small bony and fibrous bridges often have variable signal intensity (39,46). Occasionally, tiny bridges are uncovered owing to the presence of adjacent bone marrow edema, which is produced in response to focal decreased flexibility at the site of tethering (Fig 20). Radiography should not be used, as it yields overestimations of the

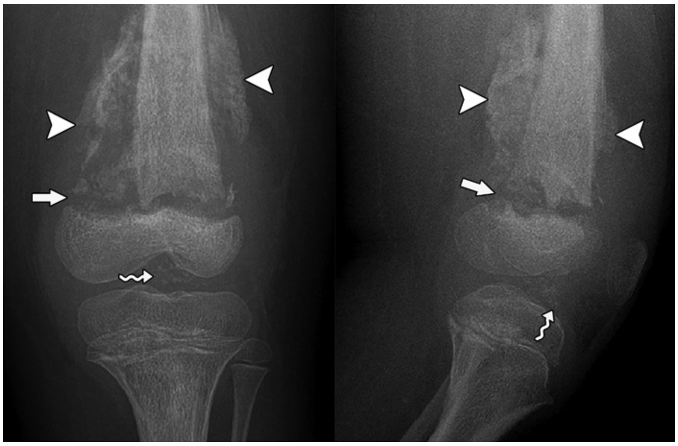

Figure 19. Chronic knee swelling in an 8-year-old boy with myelomeningocele. Anteroposterior (left) and lateral (right) knee radiographs show generalized demineralization, gracile bones, muscular atrophy, and intra-articular bodies (wavy arrows), consistent with this patient's history of a chronic neuromuscular disorder and neuropathic joint. Note the distal femur growth plate widening (straight arrows) and abundant surrounding periosteal reactions (arrowheads) as a result of repetitive, recurrent, and untreated fractures in and about the growth plate. Although it was not performed in this case, physeal biopsy often reveals an abundance of hypertrophic chondrocytes, reflecting endochondral ossification dysfunction and disorganization, in such cases.

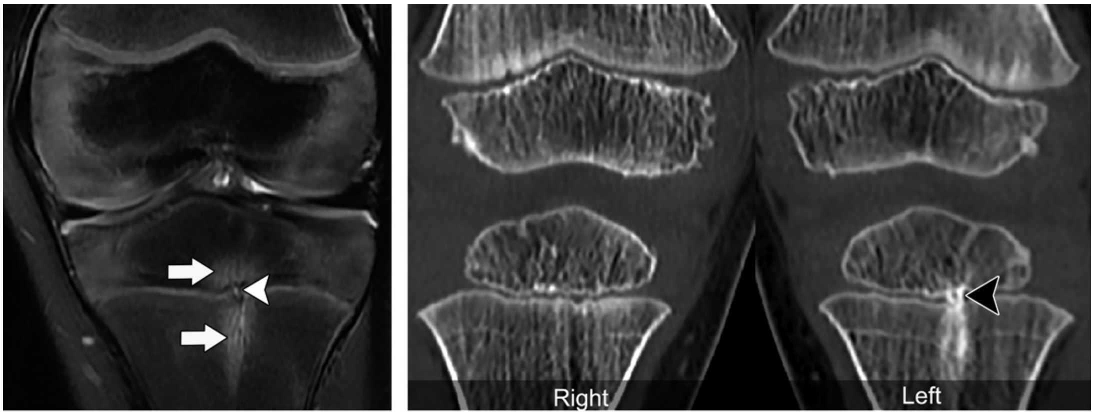

a. b.

Figure 20. Incidental small osseous bridge in a 4-year-old boy with self-limited left knee pain after a minor playground injury. **(a)** Coronal proton-density–weighted MR image with fat saturation shows a central focus of disorganized growth plate signal intensity (arrowhead) with associated focal bone marrow edema (arrows). **(b)** Findings on subsequently obtained coronal CT images confirm the presence of a tiny osseous bridge (arrowhead). Given its small size and central location, this bridge can be treated with conservative therapy and serial radiographic monitoring.

true size of the bridge in more than one-third of cases (119). These pathologic bridges should not be confused with the focal periphyseal edema (FOPE) that occurs at stereotypical sites of early physiologic growth plate closure (120) (Fig 21).

Treatment can be nonsurgical or surgical. Nonsurgical treatment is reserved for patients who are nearing skeletal maturation and have small bridges that involve less than 30% of the total growth plate area and affect the central portions of the growth plate (119,121–123). It is believed that normal physiologic forces during normal growth are sufficient to overcome these small, central osseous bridges (Fig 20) (122). Surgical treatment includes bridge resection, epiphysiodesis, and bone lengthening—all of which involve risks of infection, recurrent bridge formation, and fracture (116). Bridge resection with interposition of inert material such as fat is reserved for patients who have more than 2 years or more than 2 cm of growth remaining (123) and involvement of less than 50% of the total growth plate (43,116,119). Despite successful bridge resection, premature growth plate closure often occurs, with continued imaging and clinical monitoring required until skeletal maturation (116). Guided growth with epiphysiodesis is more appropriate for patients who have more than 50% of the physis involved or multifocal growth plate involvement that predominantly affects the peripheral portions of the growth plate. This treatment involves ipsilateral hemiepiphysiodesis to correct the angular deformity and contralateral epiphysiodesis to avoid limb length discrepancy. The goal is to prevent asymmetric growth at the expense of sacrificing the growth of the normal side. For an angular deformity that exceeds 20°, corrective osteotomy can be considered (116). Bone lengthening is reserved for patients who have a greater than 2-cm limb discrepancy or a substantial injury with minimal potential for residual growth (39). Therefore, it is important to recognize the development of growth disturbance early so that the least invasive treatment can be implemented (9,116).

Conclusion

For normal growth plate function, an orderly zonal arrangement of chondrocyte maturation and intact epiphyseal and metaphyseal vascularity are required. Injury to any or all three components of the growth plate complex (ie, growth plate, epiphysis, and metaphysis) can lead to a variety of growth disturbances that have characteristic imaging appearances and necessitate specific treatments.

Acknowledgment.—The authors thank Carol Dizack for creating the anatomic drawings.

Disclosures of Conflicts of Interest.—A.C.M. *Activities related to the present article:* disclosed no relevant relationships. *Activities not related to the present article:* personal fees from Elsevier for work on educational products. *Other activities:* disclosed no relevant relationships.

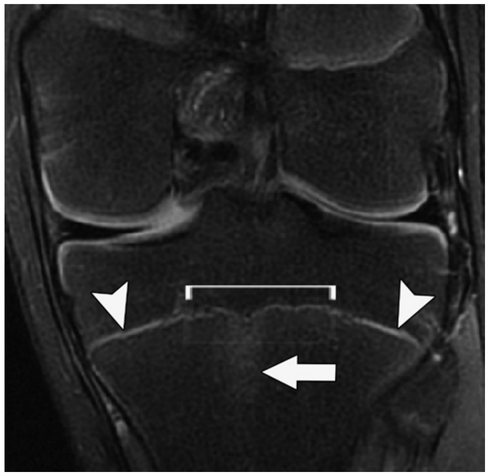

Figure 21. Focal periphyseal edema in a 17-year-old boy with an asymptomatic and healing trochlear osteochondritis dissecans. Coronal proton-density–weighted fat-saturated MR image shows the start of physiologic proximal tibial growth plate closure centrally, with narrowing and a decreased hyperintense signal (bracket). This is in contrast to the more peripheral open growth plate (arrowheads). Often, there is associated subtle bone marrow edema (arrow), which has been postulated to reflect a stress response to focally increased rigidity.

References

1. Oestreich AE. The acrophysis: a unifying concept for understanding enchondral bone growth and its disorders. II. Abnormal growth. Skeletal Radiol 2004;33(3):119–128.
2. Laor T, Jaramillo D. MR imaging insights into skeletal maturation: what is normal? Radiology 2009;250(1):28–38.
3. Ecklund K, Jaramillo D. Imaging of growth disturbance in children. Radiol Clin North Am 2001;39(4):823–841.
4. Iannotti JP. Growth plate physiology and pathology. Orthop Clin North Am 1990;21(1):1–17.
5. Brighton CT. The growth plate. Orthop Clin North Am 1984;15(4):571–595.
6. Rivas R, Shapiro F. Structural stages in the development of the long bones and epiphyses: a study in the New Zealand white rabbit. J Bone Joint Surg Am 2002;84-A(1):85–100.
7. Ogden JA. Injury to the growth mechanisms of the immature skeleton. Skeletal Radiol 1981;6(4):237–253.
8. Jaramillo D, Kammen BF, Shapiro F. Cartilaginous path of physeal fracture-separations: evaluation with MR imaging—an experimental study with histologic correlation in rabbits. Radiology 2000;215(2):504–511.
9. Rogers LF, Poznanski AK. Imaging of epiphyseal injuries. Radiology 1994;191(2):297–308.
10. Byers S, Moore AJ, Byard RW, Fazzalari NL. Quantitative histomorphometric analysis of the human growth plate from birth to adolescence. Bone 2000;27(4):495–501.
11. Hajdu S, Schwendenwein E, Kaltenecker G, et al. Growth potential of different zones of the growth plate: an experimental study in rabbits. J Orthop Res 2012;30(1):162–168.
12. Oestreich AE, Ahmad BS. The periphysis and its effect on the metaphysis. I. Definition and normal radiographic pattern. Skeletal Radiol 1992;21(5):283–286.
13. Jaramillo D, Shapiro F. Growth cartilage: normal appearance, variants and abnormalities. Magn Reson Imaging Clin N Am 1998;6(3):455–471.
14. Nguyen JC, Lee KS, Thapa MM, Rosas HG. US evaluation of juvenile idiopathic arthritis and osteoarticular infection. RadioGraphics 2017;37(4):1181–1201.
15. Laor T, Hartman AL, Jaramillo D. Local physeal widening on MR imaging: an incidental finding suggesting prior metaphyseal insult. Pediatr Radiol 1997;27(8):654–662.
16. Blumer MJ, Longato S, Fritsch H. Structure, formation and role of cartilage canals in the developing bone. Ann Anat 2008;190(4):305–315.
17. Ogden JA, Lister G. The pathology of neonatal osteomyelitis. Pediatrics 1975;55(4):474–478.
18. Barnewolt CE, Shapiro F, Jaramillo D. Normal gadolinium-enhanced MR images of the developing appendicular skeleton. I. Cartilaginous epiphysis and physis. AJR Am J Roentgenol 1997;169(1):183–189.
19. Jaimes C, Chauvin NA, Delgado J, Jaramillo D. MR imaging of normal epiphyseal development and common epiphyseal disorders. RadioGraphics 2014;34(2):449–471.
20. Jaramillo D, Laor T, Hoffer FA, et al. Epiphyseal marrow in infancy: MR imaging. Radiology 1991;180(3):809–812.
21. Chan BY, Gill KG, Rebsamen SL, Nguyen JC. MR imaging of pediatric bone marrow. RadioGraphics 2016;36(6):1911–1930.
22. Ogden JA. Growth slowdown and arrest lines. J Pediatr Orthop 1984;4(4):409–415.
23. Hynes D, O'Brien T. Growth disturbance lines after injury of the distal tibial physis: their significance in prognosis. J Bone Joint Surg Br 1988;70(2):231–233.
24. Smith BG, Rand F, Jaramillo D, Shapiro F. Early MR imaging of lower-extremity physeal fracture-separations: a preliminary report. J Pediatr Orthop 1994;14(4):526–533.
25. Thapa MM, Iyer RS, Khanna PC, Chew FS. MRI of pediatric patients. I. Normal and abnormal cartilage. AJR Am J Roentgenol 2012;198(5):W450–W455.
26. Jaramillo D, Villegas-Medina OL, Doty DK, et al. Gadolinium-enhanced MR imaging demonstrates abduction-caused hip ischemia and its reversal in piglets. AJR Am J Roentgenol 1996;166(4):879–887.
27. Jaramillo D, Villegas-Medina OL, Doty DK, et al. Age-related vascular changes in the epiphysis, physis, and metaphysis: normal findings on gadolinium-enhanced MRI of piglets. AJR Am J Roentgenol 2004;182(2):353–360.
28. Gruber HE, Lachman RS, Rimoin DL. Quantitative histology of cartilage vascular canals in the human rib: findings in normal neonates and children and in achondrogenesis II-hypochondrogenesis. J Anat 1990;173:69–75.
29. Borsa JJ, Peterson HA, Ehman RL. MR imaging of physeal bars. Radiology 1996;199(3):683–687.
30. Sailhan F, Chotel F, Guibal AL, et al. Three-dimensional MR imaging in the assessment of physeal growth arrest. Eur Radiol 2004;14(9):1600–1608.
31. Mizuta T, Benson WM, Foster BK, Paterson DC, Morris LL. Statistical analysis of the incidence of physeal injuries. J Pediatr Orthop 1987;7(5):518–523.
32. Carter SR, Aldridge MJ, Fitzgerald R, Davies AM. Stress changes of the wrist in adolescent gymnasts. Br J Radiol 1988;61(722):109–112.
33. Wu M, Fallon R, Heyworth BE. Overuse injuries in the pediatric population. Sports Med Arthrosc Rev 2016;24(4):150–158.

34. Peterson HA, Madhok R, Benson JT, Ilstrup DM, Melton LJ 3rd. Physeal fractures. I. Epidemiology in Olmsted County, Minnesota, 1979–1988. J Pediatr Orthop 1994;14(4): 423–430.
35. Caine D, DiFiori J, Maffulli N. Physeal injuries in children's and youth sports: reasons for concern? Br J Sports Med 2006;40(9):749–760.
36. Shapiro F. Epiphyseal growth plate fracture-separations: a pathophysiologic approach. Orthopedics 1982;5(6):720–736.
37. Jaramillo D, Shapiro F, Hoffer FA, et al. Posttraumatic growth-plate abnormalities: MR imaging of bony-bridge formation in rabbits. Radiology 1990;175(3):767–773.
38. Riseborough EJ, Barrett IR, Shapiro F. Growth disturbances following distal femoral physeal fracture-separations. J Bone Joint Surg Am 1983;65(7):885–893.
39. Jaramillo D, Hoffer FA, Shapiro F, Rand F. MR imaging of fractures of the growth plate. AJR Am J Roentgenol 1990;155(6):1261–1265.
40. Ogden JA, Ganey T, Light TR, Southwick WO. The pathology of acute chondro-osseous injury in the child. Yale J Biol Med 1993;66(3):219–233.
41. Lee KE, Pelker RR, Rudicel SA, Ogden JA, Panjabi MM. Histologic patterns of capital femoral growth plate fracture in the rabbit: the effect of shear direction. J Pediatr Orthop 1985;5(1):32–39.
42. Peterson HA. Physeal fractures. III. Classification. J Pediatr Orthop 1994;14(4):439–448.
43. Peterson HA. Partial growth plate arrest and its treatment. J Pediatr Orthop 1984;4(2):246–258.
44. Ogden JA. Skeletal growth mechanism injury patterns. J Pediatr Orthop 1982;2(4):371–377.
45. Barmada A, Gaynor T, Mubarak SJ. Premature physeal closure following distal tibia physeal fractures: a new radiographic predictor. J Pediatr Orthop 2003;23(6):733–739.
46. Ecklund K, Jaramillo D. Patterns of premature physeal arrest: MR imaging of 111 children. AJR Am J Roentgenol 2002;178(4):967–972.
47. Jaramillo D, Laor T, Zaleske DJ. Indirect trauma to the growth plate: results of MR imaging after epiphyseal and metaphyseal injury in rabbits. Radiology 1993;187(1):171–178.
48. Shi DP, Zhu SC, Li Y, Zheng J. Epiphyseal and physeal injury: comparison of conventional radiography and magnetic resonance imaging. Clin Imaging 2009;33(5):379–383.
49. Petit P, Panuel M, Faure F, et al. Acute fracture of the distal tibial physis: role of gradient-echo MR imaging versus plain film examination. AJR Am J Roentgenol 1996;166(5):1203–1206.
50. Lohman M, Kivisaari A, Kallio P, Puntila J, Vehmas T, Kivisaari L. Acute paediatric ankle trauma: MRI versus plain radiography. Skeletal Radiol 2001;30(9):504–511.
51. Carey J, Spence L, Blickman H, Eustace S. MRI of pediatric growth plate injury: correlation with plain film radiographs and clinical outcome. Skeletal Radiol 1998;27 (5):250–255.
52. White PG, Mah JY, Friedman L. Magnetic resonance imaging in acute physeal injuries. Skeletal Radiol 1994;23(8): 627–631.
53. Wirth T, Byers S, Byard RW, Hopwood JJ, Foster BK. The implantation of cartilaginous and periosteal tissue into growth plate defects. Int Orthop 1994;18(4):220–228.
54. Phieffer LS, Meyer RA Jr, Gruber HE, Easley M, Wattenbarger JM. Effect of interposed periosteum in an animal physeal fracture model. Clin Orthop Relat Res 2000;(376): 15–25.
55. Brenkel IJ, Dias JJ, Davies TG, Iqbal SJ, Gregg PJ. Hormone status in patients with slipped capital femoral epiphysis. J Bone Joint Surg Br 1989;71(1):33–38.
56. Umans H, Liebling MS, Moy L, Haramati N, Macy NJ, Pritzker HA. Slipped capital femoral epiphysis: a physeal lesion diagnosed by MRI, with radiographic and CT correlation. Skeletal Radiol 1998;27(3):139–144.
57. Agamanolis DP, Weiner DS, Lloyd JK. Slipped capital femoral epiphysis: a pathological study. I. A light microscopic and histochemical study of 21 cases. J Pediatr Orthop 1985;5(1):40–46.
58. Ippolito E, Mickelson MR, Ponseti IV. A histochemical study of slipped capital femoral epiphysis. J Bone Joint Surg Am 1981;63(7):1109–1113.
59. Mickelson MR, Ponseti IV, Cooper RR, Maynard JA. The ultrastructure of the growth plate in slipped capital femoral epiphysis. J Bone Joint Surg Am 1977;59(8):1076–1081.
60. Agamanolis DP, Weiner DS, Lloyd JK. Slipped capital femoral epiphysis: a pathological study. II. An ultrastructural study of 23 cases. J Pediatr Orthop 1985;5(1):47–58.
61. Ippolito E, Bellocci M, Farsetti P, Tudisco C, Perugia D. An ultrastructural study of slipped capital femoral epiphysis: pathogenetic considerations. J Orthop Res 1989;7 (2):252–259.
62. Adamczyk MJ, Weiner DS, Nugent A, McBurney D, Horton WE Jr. Increased chondrocyte apoptosis in growth plates from children with slipped capital femoral epiphysis. J Pediatr Orthop 2005;25(4):440–444.
63. Loder RT. What is the cause of avascular necrosis in unstable slipped capital femoral epiphysis and what can be done to lower the rate? J Pediatr Orthop 2013;33(1 suppl 1):S88–S91.
64. Staatz G, Honnef D, Kochs A, et al. Evaluation of femoral head vascularization in slipped capital femoral epiphysis before and after cannulated screw fixation with use of contrast-enhanced MRI: initial results. Eur Radiol 2007;17(1):163–168.
65. Lalaji A, Umans H, Schneider R, Mintz D, Liebling MS, Haramati N. MRI features of confirmed "pre-slip" capital femoral epiphysis: a report of two cases. Skeletal Radiol 2002;31(6):362–365.
66. Roaten J, Spence DD. Complications related to the treatment of slipped capital femoral epiphysis. Orthop Clin North Am 2016;47(2):405–413.
67. Kim HK. Legg-Calvé-Perthes disease. J Am Acad Orthop Surg 2010;18(11):676–686.
68. McCarthy RE. Avascular necrosis of the femoral head in children. Instr Course Lect 1988;37:59–65.
69. Ponseti IV. Legg-Perthes disease: observations on pathological changes in two cases. J Bone Joint Surg Am 1956;38-A(4):739–750.
70. Ponseti IV, Maynard JA, Weinstein SL, Ippolito EG, Pous JG. Legg-Calvé-Perthes disease: histochemical and ultrastructural observations of the epiphyseal cartilage and physis. J Bone Joint Surg Am 1983;65(6):797–807.
71. Kim HK, Skelton DN, Quigley EJ. Pathogenesis of metaphyseal radiolucent changes following ischemic necrosis of the capital femoral epiphysis in immature pigs: a preliminary report. J Bone Joint Surg Am 2004;86-A(1):129–135.
72. O'Brien T, Millis MB, Griffin PP. The early identification and classification of growth disturbances of the proximal end of the femur. J Bone Joint Surg Am 1986;68(7): 970–980.
73. Park KW, Rejuso CA, Cho WT, Song HR. Timing of premature physeal closure in Legg-Calve-Perthes Disease. Int Orthop 2014;38(10):2137–2142.
74. Ha AS, Wells L, Jaramillo D. Importance of sagittal MR imaging in nontraumatic femoral head osteonecrosis in children. Pediatr Radiol 2008;38(11):1195–1200.
75. de Sanctis N. Magnetic resonance imaging in Legg-Calvè-Perthes disease: review of literature. J Pediatr Orthop 2011;31(2 suppl):S163–S167.
76. Bowen JR, Schreiber FC, Foster BK, Wein BK. Premature femoral neck physeal closure in Perthes' disease. Clin Orthop Relat Res 1982;(171):24–29.
77. Joseph B. Natural history of early onset and late-onset Legg-Calve-Perthes disease. J Pediatr Orthop 2011;31(2 suppl):S152–S155.
78. Joseph B, Varghese G, Mulpuri K, Narasimha Rao K, Nair NS. Natural evolution of Perthes disease: a study of 610 children under 12 years of age at disease onset. J Pediatr Orthop 2003;23(5):590–600.
79. Jaramillo D, Kasser JR, Villegas-Medina OL, Gaary E, Zurakowski D. Cartilaginous abnormalities and growth disturbances in Legg-Calvé-Perthes disease: evaluation with MR imaging. Radiology 1995;197(3):767–773.
80. de Sanctis N, Rega AN, Rondinella F. Prognostic evaluation of Legg-Calvé-Perthes disease by MRI. I. The role of physeal involvement. J Pediatr Orthop 2000;20(4):455–462.
81. Larsen EH, Reimann I. Calvé Perthes disease with special reference to histological observations. Acta Orthop Scand 1973;44(4):426–438.

82. Stevens PM, Anderson LA, Gililland JM, Novais E. Guided growth of the trochanteric apophysis combined with soft tissue release for Legg-Calve-Perthes disease. Strateg Trauma Limb Reconstr 2014;9(1):37–43.
83. Rosenbaum DG, Servaes S, Bogner EA, Jaramillo D, Mintz DN. MR imaging in postreduction assessment of developmental dysplasia of the hip: goals and obstacles. RadioGraphics 2016;36(3):840–854.
84. Jaramillo D, Villegas-Medina OL, Doty DK, et al. Gadolinium-enhanced MR imaging demonstrates abduction-caused hip ischemia and its reversal in piglets. Pediatr Radiol 1995;25(8):578–587.
85. Yousefzadeh DK, Jaramillo D, Johnson N, Doerger K, Sullivan C. Biphasic threat to femoral head perfusion in abduction: arterial hypoperfusion and venous congestion. Pediatr Radiol 2010;40(9):1517–1525.
86. Jaramillo D, Villegas-Medina O, Laor T, Shapiro F, Millis MB. Gadolinium-enhanced MR imaging of pediatric patients after reduction of dysplastic hips: assessment of femoral head position, factors impeding reduction, and femoral head ischemia. AJR Am J Roentgenol 1998;170(6):1633–1637.
87. Salter RB, Kostuik J, Dallas S. Avascular necrosis of the femoral head as a complication of treatment for congenital dislocation of the hip in young children: a clinical and experimental investigation. Can J Surg 1969;12(1):44–61.
88. Keret D, MacEwen GD. Growth disturbance of the proximal part of the femur after treatment for congenital dislocation of the hip. J Bone Joint Surg Am 1991;73(3):410–423.
89. Claessen FM, Louwerens JK, Doornberg JN, van Dijk CN, van den Bekerom MP, Eygendaal D. Hegemann's disease and fishtail deformity: aetiopathogenesis, radiographic appearance and clinical outcome. J Child Orthop 2015;9(1):1–8.
90. Otsuka J, Horii E, Koh S, Hiroishi M. Unusual humeral medial condyle fracture in an adolescent because of a previous post-traumatic fishtail deformity: a case report. J Pediatr Orthop B 2015;24(5):408–411.
91. Narayanan S, Shailam R, Grottkau BE, Nimkin K. Fishtail deformity: a delayed complication of distal humeral fractures in children. Pediatr Radiol 2015;45(6):814–819.
92. Glotzbecker MP, Bae DS, Links AC, Waters PM. Fishtail deformity of the distal humerus: a report of 15 cases. J Pediatr Orthop 2013;33(6):592–597.
93. Kimball JP, Glowczewskie F, Wright TW. Intraosseous blood supply to the distal humerus. J Hand Surg Am 2007;32(5):642–646.
94. Rivero SM, Zhao C, Sabharwal S. Are patient demographics different for early-onset and late-onset Blount disease? results based on meta-analysis. J Pediatr Orthop B 2015;24(6):515–520.
95. Jaramillo D, Hoffer FA. Cartilaginous epiphysis and growth plate: normal and abnormal MR imaging findings. AJR Am J Roentgenol 1992;158(5):1105–1110.
96. Arai K, Haga N, Taniguchi K, Nakamura K. Magnetic resonance imaging findings and treatment outcome in late-onset tibia vara. J Pediatr Orthop 2001;21(6):808–811.
97. Langenskiöld A. Growth disturbance after osteomyelitis of femoral condyles in infants. Acta Orthop Scand 1984;55(1):1–13.
98. Gilbertson-Dahdal D, Wright JE, Krupinski E, McCurdy WE, Taljanovic MS. Transphyseal involvement of pyogenic osteomyelitis is considerably more common than classically taught. AJR Am J Roentgenol 2014;203(1):190–195.
99. O'Sullivan ME, Fogarty EE. Distal tibial physeal arrest: a complication of meningococcal septicemia. J Pediatr Orthop 1990;10(4):549–550.
100. Kruse RW, Tassanawipas A, Bowen JR. Orthopedic sequelae of meningococcemia. Orthopedics 1991;14(2):174–178.
101. Appel M, Pauleto AC, Cunha LA. Osteochondral sequelae of meningococcemia: radiographic aspects. J Pediatr Orthop 2002;22(4):511–516.
102. Grogan DP, Love SM, Ogden JA, Millar EA, Johnson LO. Chondro-osseous growth abnormalities after meningococcemia: a clinical and histopathological study. J Bone Joint Surg Am 1989;71(6):920–928.
103. Peters W, Irving J, Letts M. Long-term effects of neonatal bone and joint infection on adjacent growth plates. J Pediatr Orthop 1992;12(6):806–810.
104. Trueta J, Amato VP. The vascular contribution to osteogenesis. III. Changes in the growth cartilage caused by experimentally induced ischaemia. J Bone Joint Surg Br 1960;42-B:571–587.
105. Kleinman PK. Diagnostic imaging in infant abuse. AJR Am J Roentgenol 1990;155(4):703–712.
106. Merrow AC, Laor T. Leukemia and treatment: imprint on the growing skeleton. Pediatr Radiol 2008;38(5):594.
107. Roy S, Caine D, Singer KM. Stress changes of the distal radial epiphysis in young gymnasts: a report of twenty-one cases and a review of the literature. Am J Sports Med 1985;13(5):301–308.
108. Caine D, Roy S, Singer KM, Broekhoff J. Stress changes of the distal radial growth plate: a radiographic survey and review of the literature. Am J Sports Med 1992;20(3):290–298.
109. DiFiori JP, Puffer JC, Mandelbaum BR, Dorey F. Distal radial growth plate injury and positive ulnar variance in nonelite gymnasts. Am J Sports Med 1997;25(6):763–768.
110. De Smet L, Claessens A, Lefevre J, Beunen G. Gymnast wrist: an epidemiologic survey of ulnar variance and stress changes of the radial physis in elite female gymnasts. Am J Sports Med 1994;22(6):846–850.
111. De Smet L, Claessens A, Fabry G. Gymnast wrist. Acta Orthop Belg 1993;59(4):377–380.
112. Chauhan DK, Dhillon MS, Tripathy SK. Neuro-epiphyseal injury around the ankle: a case report. Foot 2009;19(2):133–136.
113. Khoury JG, Morcuende JA. Dramatic subperiosteal bone formation following physeal injury in patients with myelomeningocele. Iowa Orthop J 2002;22:94–98.
114. Roberts JA, Bennet GC, MacKenzie JR. Physeal widening in children with myelomeningocele. J Bone Joint Surg Br 1989;71(1):30–32.
115. Langenskiöld A. Surgical treatment of partial closure of the growth plate. J Pediatr Orthop 1981;1(1):3–11.
116. Kasser JR. Physeal bar resections after growth arrest about the knee. Clin Orthop Relat Res 1990;(255):68–74.
117. Gabel GT, Peterson HA, Berquist TH. Premature partial physeal arrest: diagnosis by magnetic resonance imaging in two cases. Clin Orthop Relat Res 1991;(272):242–247.
118. Lurie B, Koff MF, Shah P, et al. Three-dimensional magnetic resonance imaging of physeal injury: reliability and clinical utility. J Pediatr Orthop 2014;34(3):239–245.
119. Lohman M, Kivisaari A, Vehmas T, Kallio P, Puntila J, Kivisaari L. MRI in the assessment of growth arrest. Pediatr Radiol 2002;32(1):41–45.
120. Zbojniewicz AM, Laor T. Focal periphyseal edema (FOPE) zone on MRI of the adolescent knee: a potentially painful manifestation of physiologic physeal fusion? AJR Am J Roentgenol 2011;197(4):998–1004.
121. Chimenti P, Hammert W. Posttraumatic distal ulnar physeal arrest: a case report and review of the literature. Hand (NY) 2013;8(1):115–119.
122. Kennon JC, Ganey TM, Gaston RG, Ogden JA. Continued growth after limited physeal bridging. J Pediatr Orthop 2013;33(8):857–861.
123. Khoshhal KI, Kiefer GN. Physeal bridge resection. J Am Acad Orthop Surg 2005;13(1):47–58.